

4. COMPOSITION AND ORIGIN OF VOLCANICLASTIC SEDIMENTS IN THE LAU BASIN (SOUTHWEST PACIFIC), LEG 135 (SITES 834–839)¹

Ulrich Bednarz^{2,3} and Hans-Ulrich Schmincke²

ABSTRACT

Early Pliocene to Pleistocene volcanoclastic sediments recovered during Ocean Drilling Program Leg 135 from Sites 834 to 839 in the Lau Basin show a wide range of chemical and mineralogical compositions extending the spectrum previously known from the Lau Basin, Lau Ridge and Tofua Arc. The following major types of volcanoclastics have been distinguished: (1) primary fallout ashes originating from eruptions on land, (2) epiclastic deposits that resulted from subaerial and submarine eruptions, (3) subaqueous fallout and pyroclastic flow deposits resulting from explosive submarine eruptions, and (4) hyaloclastites resulting from mechanical fragmentation and spalling of chilled margins of submarine pillow tubes and sheet-lava flows.

Vitric shards are mostly basaltic andesitic to rhyolitic and broadly follow two major trends in terms of K₂O enrichment: a low-K series (LKS) with about 1 wt% K₂O at 70 wt% SiO₂, and a very low-K series (VLKS) with only about 0.5 wt% K₂O at 70 wt% SiO₂.

Sites 834 and 835 on "old" backarc basin crust, >4.2 and 3.4 m.y. old, comprise LKS rhyolites >3.3 m.y. old. Calc-alkaline basaltic turbidites originating from the Lau Ridge flowed in at 3.3 Ma. In the period from 3.3 to 2.4 Ma basaltic andesitic to rhyolitic, fine-grained LKS and VLKS volcanoclastics were deposited by turbidity currents and subaerial fallout. Three thin, discrete fallout layers (2.4–3.2 m.y. old) with high-K calc-alkaline compositions probably erupted in New Zealand.

Volcanoclastics from Site 836, all <0.6 m.y. old, make up 24% of the sediments and comprise local basaltic andesitic to andesitic hyaloclastites with low Ba/Zr ratios of 0.9 to 1.4 and polymict andesitic sediments with Ba/Zr ratios of up to 5.5, containing clasts altered to lower greenschist facies.

In Sites 837–839, drilled on young crust (1.8–2.1 m.y. old), volcanoclastics make up 45%–64% of the total sediment. Glass compositions are often bimodal with a mafic and a rhyolitic population. Large-volume rhyolitic, silt- to lapilli-sized volcanoclastics are interpreted as pyroclastic flows from explosive eruptions on a seamount 25–50 km away from the sites. Ba/Zr ratios are 2 to 4, partially overlapping with some Lau Basin basement lavas that show an "arc" signature, and they can reach values >5 in thin volcanoclastic layers <0.6 m.y. old.

INTRODUCTION

Volcanoclastic sediments are an important tool in reconstructing the temporal and compositional evolution and eruptive styles of volcanism when the original volcanic edifices are no longer or have never been exposed. The basis for the interpretation of chemical and petrological data must, however, be a careful reconstruction of the location of eruptive sites, styles of eruption, fragmentation, and depositional mechanisms.

Volcanoclastic sediments from Tonga Ridge, Tofua Arc, and the Lau Basin sampled within the surrounding sedimentary basins have recently attracted increasing interest, starting with Deep Sea Drilling Project (DSDP) Leg 21 (Site 203) and have been studied petrologically and geochemically in some detail (Churkin and Packham, 1973; Cawood, 1985; Exon et al., 1985; Hawkins, 1985; Vallier, O'Connor, et al., 1985; Vallier, Stevenson, and Scholl, 1985; Riech, 1990; Riech et al., 1990; von Rad and Mühe, 1990; von Rad et al., 1990). The maximum age of samples from the Lau Basin, mostly recovered by dredging and by piston and gravity coring, does not exceed 840 k.y., however. Ash layers and pumice clasts in the northern and southern Lau basins were interpreted as fallout ashes and turbidites from the remobilization of fallout ashes of low-K andesitic to rhyolitic composition and are interpreted to have originated mostly from explosive volcanism on the Tofua Volcanic Arc (von Rad and Mühe, 1990).

Drill Sites

Six sites (834–839) were drilled within the western Lau backarc basin during Leg 135 (December 1990 to February 1991), mostly by advanced hydraulic piston coring (APC), with excellent core recovery of often 100% and mostly only little disturbance of sedimentary structures. Sediment thicknesses encountered in the Lau Basin ranged from 20.20 m (Site 836) to >259 m (Site 838, where basement was not reached), with maximum ages of post-lava sediments ranging from 0.64 m.y. (Site 836) to 3.8 m.y. (Site 834). Silt- to lapilli-sized volcanoclastics occur in varying proportions in the sediments of the Lau Basin sites and make up 12% in Hole 834A, 2% in Hole 835A, 24% in Hole 836A, 59% in Hole 837A, 45% in Hole 838A, and 64% in Hole 839A. Hemipelagic, nonvolcanic sediments are clearly dominated by clayey nannofossil ooze in all Lau Basin sites.

Major objectives for the cruise were to understand the timing and early history of opening of the Lau Basin, to sample the Lau Basin floor more representative than before, and to look for possible relations between magmatic and tectonic processes in the arc and backarc basins (Leg 135 Shipboard Scientific Party, 1991).

Sites 834 and 835 are located in the westernmost part of the Lau basin within two separate, small, elongate, north-trending, sediment-filled sub-basins, at distances of only 80 and 130 km from the center of the (remnant arc) Lau Ridge (Fig. 1).

Sites 836 to 839, clustered in an area of about 100 × 50 km, about 220 km to the southeast of Sites 834 and 835, were drilled directly west of the Eastern Lau Spreading Center (ELSC). They are located in three fault-bounded sedimentary sub-basins, with basement ages ranging from 0.6 (Site 836) to 2.1 m.y. (Site 837).

Early Pliocene volcanoclastics of about 3.8 m.y. from Site 834 are the oldest post-lava volcanic sediments from the Lau Basin recovered during the cruise, whereas volcanic input <0.6 m.y. was generally poor (with the exception of Site 836).

¹ Hawkins, J., Parson, L., Allan, J., et al., 1994. *Proc. ODP, Sci. Results*, 135: College Station, TX (Ocean Drilling Program).

² GEOMAR, Wischhofstraße 1-3, D-24148 Kiel 14, Federal Republic of Germany.

³ Present address: Das Baugrund Institut, Broßhauser Strasse 27, D-42697 Solingen 11, Federal Republic of Germany.

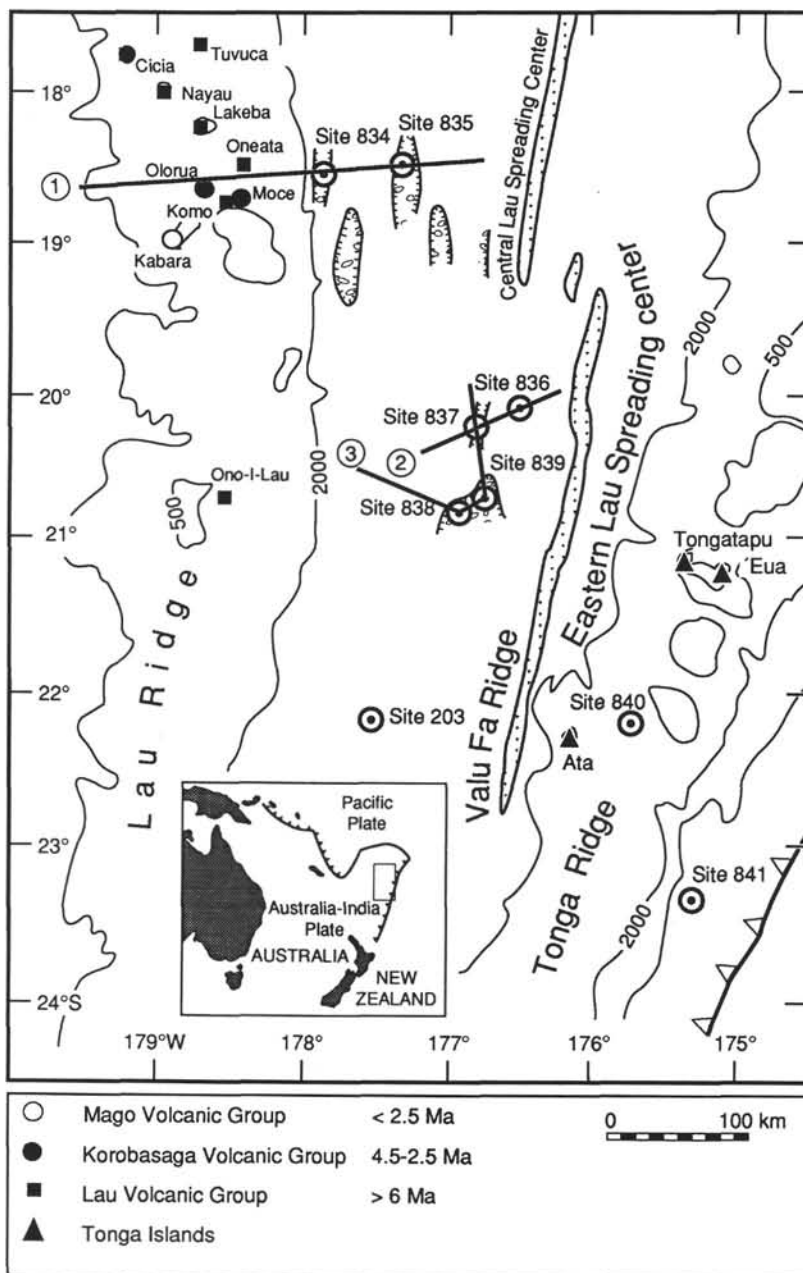


Figure 1. Simplified structural and bathymetric map of the southern Lau Basin (redrawn after Parson, Hawkins, Allan, et al., 1992). Profiles 1, 2, and 3 are also indicated. Distribution of volcanic rocks on Lau Islands after Woodhall (1985).

Types of Volcaniclastic Deposits

Primary subaerial fallout tephra (ashes), are mostly not redeposited. Some show gravitational sorting according to grain size and densities of particles caused by settling through the water column. Some thin layers interbedded in nanofossil ooze are disrupted by bioturbation. Some are redeposited in their medial and distal facies where deposited on submarine slopes. The components of individual layers may vary widely in composition. They will, however, belong to a single magmatic series, except for xenolithic and accidental material incorporated during the eruption. Phenocryst modes are close to primary (e.g., ranging from 5 to 10 vol%), whereas igneous

minerals in mass-flow deposits are mostly either completely removed (<1 vol%) or strongly enriched (30–50 vol%).

Epiclastic deposits that presumably resulted from subaerial to shallow submarine eruptions on the margins of the Lau Basin (Tonga Ridge, Tofua Arc) are redeposited by turbidites and other mass gravity flows on a local to regional scale. They may have the compositional characteristics of primary deposits when genetically directly related to individual eruptions, but they may also be heterogeneous, incorporating a wide range of erosional detritus. Most distinctive for identification is the occurrence of erosive bases and more rarely cross-bedding and laminar bedding. Many epiclastic deposits consist of well-sorted beds that show a distinct grain-size grading. Zones of high

concentrations of volcanoclastic material (80–100 vol%) may be restricted to the basal 15%–25% of individual units whereas the upper portions grade into hemipelagic sediments. Some epiclastic deposits have well-developed grain-size and compositional grading and show water-escape structures.

Little is known about eruption and emplacement mechanisms, dispersal patterns, and related sedimentary structures of highly evolved tephra resulting from explosive deep submarine eruptions. We assume that they form subaqueous fallout deposits and subaqueous pyroclastic flow deposits analogous to subaerial eruptions. Pyroclastic flows are probably more common as most tephra is likely transported to more distal locations during the eruption either because of unstable accumulation of large tephra volumes close to the vent area or because of eruption and/or deposition on steep slopes. Subaqueous pyroclastic flows are difficult to distinguish from compositionally homogeneous epiclastic deposits. In the proximal facies, when channelized in small basins also in more distal locations, they are characterized by large thicknesses of individual depositional units (up to several tens of meters) and diameters of pumice clasts in the lapilli and block range (>64 mm) in the basal parts of depositional units. In the proximal facies, well-developed water-escape structures in the underlying hemipelagic deposits are probably more common than in pure epiclastic deposits because of extreme deposition rates and thick accumulations of tephra.

Hyaloclastites resulting from mechanical fragmentation and spalling of chilled margins and rinds of active submarine pillow tubes and sheet-lava flows may be redeposited on a local scale but they can rather be used as proximity indicators for volcanic activity. They are normally chemically and petrologically homogeneous, predominantly in the mafic and intermediate compositional range. Vitric clasts and shards are characterized by the dominance of angular and blocky morphologies. When microlitic groundmass crystals have been developed, they generally show fluidal textures.

Pumice lapilli resulting from the slow submergence of individual clasts from drifting pumice rafts, originating from shallow submarine or near-shore subaerial eruptions, occur in varying abundance isolated in all hemipelagic sediments of the Lau Basin. They will not be discussed further in this study.

ANALYTICAL METHODS

Fifty-one unconsolidated volcanoclastic samples from Sites 834 to 839 were separated by wet sieving (2 and 1 mm and 500, 250, 125, and 63 μm) and ultrasonic sieving (40, 30, and 20 μm) for grain-size distributions and preparation of samples for chemical analyses (Table 1).

Seventy bulk-rock samples of selected grain-size fractions were analyzed on glass fusion beads by X-ray fluorescence spectrometry (XRF), using a fully automated Philips PW 1480 spectrometer, running on a Rh-tube with the analytical program OXIQUANT (calibrated on 270 international geologic and synthetic standards) for major and 24 trace elements (Table 2). The 2σ error for Zr is 4.4 ppm (detection limit: 1 ppm), 21.3 ppm for Ba (detection limit: 14 ppm), and 4.6 ppm for Nd (detection limit: 6 ppm). Values for Mo, Nb, Th, U and rare earth elements (REE) are not reported because they are low and close to the detection limit and/or the 2σ errors. Two grain-size fractions were analyzed separately for comparison in some samples from Holes 837A, 838A, and 839A (see downhole plots below). Variations were mostly insignificant, rare larger differences are a result of the dominance of igneous minerals in certain grain-size fractions and as well as a result of the frequent compositional bimodality of the glasses. The more mafic, denser glasses are generally more abundant in the smaller grain-size fractions.

The fusion beads consist of rock powders (prepared in an agate mill and dried at 100°C overnight) and flux (lithium tetraborate, Johnson Matthey Spectroflux 100) in the ratio 1:6. Samples are pre-oxidized with ammonium-nitrate for 15 min at 500°C, melted at 1200°C for 12 min and finally poured into a 32-mm diameter Pt-pellet mold.

Table 1. Grain-size characteristics of selected unconsolidated volcanoclastic samples from Sites 834–839 obtained by sieve analyses.

Core, Section, Interval (cm)	Depth (mbsf)	Age (ka)	Median (Φ)	Median (mm)	Skewness	Sorting (Φ)
135-834A-						
5H-5, 76-78 cm	42.85	2350	4.77	0.037	-0.66	NA
6H-2, 36-37 cm	47.48	2700	4.70	0.038	-0.07	1.17
6H-7, 33-35 cm	55.00	2850	4.59	0.042	-0.02	0.54
7H-4, 64-65 cm	60.29	3050	4.73	0.038	0.06	0.44
8H-3, 118-120 cm	67.64	3300	3.20	0.109	0.93	1.63
8H-4, 33-35 cm	69.56	3300	2.13	0.228	0.63	0.69
9H-6, 101-103 cm	82.69	3600	3.79	0.072	0.58	0.97
12X-1, 65-67 cm	103.57	3800	4.73	0.038	0.21	1.08
135-835A-						
5H-6, 73-76 cm	46.23	650	4.85	0.035	0.14	1.09
8H-6, 32-34 cm	74.32	1980	4.52	0.044	-0.10	1.66
9H-2, 50-52 cm	78.02	1985	2.86	0.138	0.96	3.03
15H-6, 71-73 cm	141.39	3120	2.38	0.192	0.57	0.89
135-836A-						
2H-4, 91-93 cm	6.64	261	3.74	0.075	0.40	1.71
2H-6, 39-41 cm	9.10	361	4.77	0.037	0.02	1.34
3H-3, 68-70 cm	14.69	529	0.11	0.927	0.42	1.11
3H-4, 29-31 cm	17.05	561	3.77	0.073	0.21	1.38
135-837A-						
1H-5, 84-86 cm	6.84	343	4.94	0.033	-0.14	1.11
2H-6, 120-122 cm	16.70	554	5.23	0.027	0.20	0.56
3H-1, 89-91 cm	18.39	568	2.76	0.148	0.07	1.05
3H-3, 32-34 cm	20.82	587	4.78	0.036	0.24	0.82
4H-2, 122-124 cm	29.72	1459	5.16	0.028	0.04	0.56
5H-5, 17-19 cm	42.67	1605	5.05	0.030	0.08	0.67
6H-5, 1-3 cm	52.01	1605	2.23	0.213	0.35	0.89
6H-5, 22-24 cm	52.22	1605	1.79	0.289	0.08	1.50
7H-2, 140-142 cm	58.40	1654	4.03	0.061	0.57	1.61
8H-1, 56-58 cm	65.56	1732	1.74	0.299	0.43	0.83
8H-113-115 cm	70.63	1825	4.62	0.041	0.32	0.96
9H-3, 44-46 cm	77.94	2059	1.61	0.328	0.52	0.47
135-838A-						
2H-3, 147-149 cm	8.17	502	5.33	0.025	-0.27	n.a.
3H-2, 141-143 cm	16.11	583	1.95	0.259	0.70	1.11
4H-3, 100-102 cm	26.70	856	1.15	0.451	0.70	0.99
4H-5, 59-61 cm	29.29	933	1.20	0.435	0.53	0.80
5H-3, 88-90 cm	36.08	1186	1.61	0.328	0.44	1.29
5H-7, 40-42 cm	41.60	1295	1.92	0.264	0.78	0.98
6H-5, 53-55 cm	48.23	1559	0.28	0.824	0.59	1.66
7H-6, 46-48 cm	59.16	1732	-0.73	1.659	1.25	2.58
8H-6, 74-76 cm	68.94	1762	-1.51	2.848	1.41	2.17
9H-2, 139-142 cm	73.09	1798	1.23	0.426	0.46	1.04
9H-3, 9-12 cm	73.29	1798	1.12	0.460	0.55	1.23
11H-6, 39-41 cm	97.09	1921	-0.78	1.717	0.78	1.01
135-839A-						
1H-3, 30-32 cm	3.30	366	5.05	0.030	0.33	0.50
2H-1, 39-41 cm	4.89	502	5.00	0.031	0.06	0.48
3H-6, 140-142 cm	22.90	754	4.78	0.036	-0.89	0.43
4H-4, 110-112 cm	29.10	754	1.98	0.253	0.30	1.10
5H-3, 129-131 cm	37.29	1031	2.52	0.174	0.32	0.78
6H-6, 42-44 cm	50.42	1618	4.66	0.040	-0.19	1.08
7H-6, 129-131 cm	60.79	1685	3.60	0.082	0.27	1.33
9H-2, 129-131 cm	73.79	1714	3.29	0.102	0.02	0.80
10H-4, 102-104 cm	86.02	1714	-1.08	2.114	0.82	1.51
11H-6, 95-97 cm	98.45	1728	2.52	0.174	0.37	0.76
15X-1, 44-46 cm	128.94	1763	4.90	0.033	0.27	0.30
21X-CC, 36-38 cm	186.56	1828	1.77	0.293	0.64	1.61

Note: NA = not analyzed.

Table 2. Representative selected electron microprobe analyses of fresh vitric shards from Sites 834–838.

Hole	834A														
Core	5					6					7				
Type	H														
Section	5			2			7			4			5		
Top	76			36			33			64			101		
Bottom	78			3			35			65			103		
Measuring point	5	9	11	86	69	66	29	32	30	46	39	55			
Depth (mbsf)	42.85			47.48			55.00			60.29			62.15		
Age (ka)	2350			2700			2850			3050			3100		
SiO ₂	74.70	73.29	72.79	60.28	67.85	72.31	59.40	69.29	71.52	67.42	72.87	71.43			
TiO ₂	0.18	0.17	0.17	1.03	0.72	0.56	0.97	0.71	0.70	0.71	0.56	0.15			
Al ₂ O ₃	13.00	12.96	12.84	14.33	13.22	12.38	14.08	11.97	12.18	12.08	12.09	12.71			
FeO	0.80	0.73	0.83	9.13	6.99	5.71	9.89	5.69	5.58	4.84	4.14	1.02			
MgO	0.13	0.11	0.13	2.41	1.21	0.67	2.81	0.99	0.87	1.00	0.72	0.20			
MnO	0.06	0.04	0.10	0.21	0.16	0.25	0.23	0.16	0.20	0.08	0.06	0.06			
CaO	0.89	0.88	0.89	6.97	5.04	4.04	7.16	4.08	4.00	4.08	3.40	0.99			
Na ₂ O	2.76	2.78	3.02	2.05	2.26	1.42	2.68	2.47	2.02	2.63	2.64	3.02			
K ₂ O	3.91	4.04	3.98	0.23	0.31	0.36	0.22	0.39	0.34	0.53	0.67	3.34			
Total	96.43	95.01	94.76	96.63	97.77	97.72	97.44	95.75	97.42	93.36	97.14	92.94			

Hole	834A														
Core	7					8					9				
Type	H														
Section	5			3			4			6					
Top	101			147			118			33			101		
Bottom	103			148			120			35			103		
Measuring point	47	60	3	15	7	38	47	26	126	125	113	66			
Depth (mbsf)	62.15			62.62			68.78			69.43			82.69		
Age (ka)	3100			3150			3300			3600					
SiO ₂	73.54	76.15	70.06	72.05	72.95	49.21	50.05	50.65	49.54	50.36	58.98	67.15			
TiO ₂	0.17	0.21	0.15	0.17	0.12	1.58	1.62	1.72	1.74	1.74	1.23	0.61			
Al ₂ O ₃	13.30	12.13	13.53	13.16	13.21	14.12	13.93	13.63	13.95	14.33	14.93	13.12			
FeO	0.92	0.96	1.05	0.89	0.73	12.62	12.95	13.41	13.37	13.09	7.37	4.31			
MgO	0.22	0.13	0.27	0.21	0.19	4.91	4.82	4.43	4.55	4.31	1.87	1.06			
MnO	0.10	0.09	0.01	0.10	0.09	0.00	0.06	0.27	0.24	0.27	0.18	0.12			
CaO	0.99	0.26	1.04	0.86	0.89	10.01	9.74	9.29	9.42	9.16	5.58	3.45			
Na ₂ O	2.25	1.09	2.98	3.07	3.17	2.48	2.56	2.51	2.69	2.76	2.70	2.31			
K ₂ O	3.30	3.80	3.28	3.60	3.88	1.52	1.50	1.65	1.45	1.61	3.71	0.92			
Total	94.80	94.84	92.38	94.11	95.23	96.44	97.22	97.57	96.94	97.62	96.56	93.05			

Note: Major elements in wt%.

Concentrations of H₂O and CO₂ were determined in 70 bulk-rock samples by infrared spectrometry, using a ROSEMOUNT CWA 5003 spectrometer (Table 2). Pulverized samples were inserted into an inert gas (N₂) purged analysis furnace at a temperature of 1000°C. Both gases (H₂O and CO₂) were analyzed at a thermostated infrared gas analyzer with a maximum resolution of 0.0001% and a relative accuracy of ±0.5%.

Concentrations of C and S were determined in 70 bulk-rock samples by infrared spectrometry, using a ROSEMOUNT CSA 5003 spectrometer (Table 2). Pulverized samples were pyrolyzed in an RF-furnace where C and S were oxidized to CO₂ and SO₂ by the flow of a technical oxygen gas. Concentrations were measured by a thermo-

Table 2 (continued).

Hole	834A					835A					836A				
Core	9					5					15				
Type	H														
Section	6			6			7			6			3		
Top	101			73			16			71			68		
Bottom	103			76			18			73			70		
Measuring point	57	60	98	90	80	123	130	127	36	33	26	9			
Depth (mbsf)	82.69			47.21			141.01			14.69					
Age (ka)	3600			650			3120			529					
SiO ₂	69.76	70.86	54.77	58.74	68.23	52.16	55.36	60.12	60.50	70.51	72.94	53.23			
TiO ₂	0.49	0.46	0.45	0.88	0.61	0.35	0.57	0.88	1.06	0.40	0.22	1.23			
Al ₂ O ₃	12.56	12.76	18.28	13.38	13.39	24.14	13.65	12.39	14.42	13.28	11.62	15.24			
FeO	3.41	3.50	8.01	10.92	6.41	5.03	11.18	11.61	9.57	5.67	3.58	10.76			
MgO	0.58	0.60	3.84	2.85	1.21	1.45	4.21	2.40	1.61	0.29	0.12	4.08			
MnO	0.01	1.87	0.04	0.01	0.08	0.23	0.14	0.15	0.22	0.17	0.13	0.22			
CaO	2.57	2.70	9.80	7.55	4.58	12.76	9.59	7.77	5.40	3.00	1.88	8.83			
Na ₂ O	2.15	2.67	2.63	2.55	2.55	2.59	1.60	2.01	2.94	2.02	1.60	2.82			
K ₂ O	1.01	0.00	0.42	0.78	1.12	0.20	0.46	0.68	0.68	1.14	1.31	0.23			
Total	92.54	95.42	98.23	97.67	98.17	98.91	96.76	98.01	96.40	96.48	93.40	96.64			

Hole	836A					838A						
Core	3					2						
Type	H											
Section	3		4			3						
Top	68		29			147						
Bottom	70		31			149						
Measuring point	3	16	8	2	1	60	52	50	41	35	25	36
Depth (mbsf)	14.69		15.70			8.18						
Age (ka)	529		543			502						
SiO ₂	54.37	56.00	52.50	54.34	55.97	55.54	56.69	58.13	48.49	52.03	70.85	73.73
TiO ₂	1.47	1.12	1.10	1.13	1.16	0.82	0.65	1.07	0.71	0.83	0.51	0.38
Al ₂ O ₃	13.80	14.41	14.47	14.31	14.27	14.21	13.16	13.30	15.30	14.69	12.53	11.62
FeO	12.70	10.63	10.72	11.06	10.63	10.65	11.01	10.89	9.33	9.76	3.03	2.21
MgO	3.52	3.17	5.09	3.62	3.37	4.08	3.92	2.93	7.37	5.88	0.70	0.43
MnO	0.21	0.22	0.19	0.23	0.25	0.15	0.20	0.15	0.22	0.15	0.06	0.06
CaO	8.00	7.64	9.64	8.08	7.88	8.98	9.40	7.60	13.17	10.71	3.36	2.32
Na ₂ O	2.87	3.05	2.73	3.05	3.10	2.21	1.73	2.52	1.65	1.98	1.77	1.73
K ₂ O	0.30	0.30	0.18	0.30	0.28	0.66	0.49	0.83	0.36	0.47	0.92	1.10
Total	97.24	96.54	96.62	96.12	96.91	97.30	97.25	97.42	96.60	96.50	93.73	93.58

stated infrared analyzer with a resolution of 0.0001% at a range of 0.001 to 100 wt% and a relative accuracy of ±1%.

Major element compositions of 340 fresh vitric shards were measured by electron microprobe in 17 selected samples from Sites 834, 835, 836, and 838, using a CAMEBAX wavelength dispersive automatic microprobe (Table 3). A defocused beam (10-µm diameter) with a beam current of 9 nA, an acceleration voltage of 15 kV, and a counting time of 20 s were used. Potassium was the first element to be measured.

Descriptions of sedimentary structures are taken from the visual core descriptions (VCDs) written and drafted by the shipboard scientific party during the cruise.

Table 2 (continued).

Hole	838A											
Core	6				8				9			
Type	H											
Section	5				6				3			
Top	53				74				9			
Bottom	55				76				12			
Measuring point	58	45	89	116	97	99	15	12	4	107	102	90
Depth (mbsf)	50.84				68.94				75.45			
Age (ka)	1559				1762				1798			
SiO ₂	50.31	51.64	59.82	70.01	71.93	73.64	51.37	70.74	74.10	51.44	52.23	52.96
TiO ₂	0.54	0.89	0.99	0.71	0.41	0.37	0.74	0.53	0.17	0.90	0.93	0.95
Al ₂ O ₃	21.25	14.62	13.85	12.25	12.56	11.20	15.14	12.47	11.60	14.10	14.29	14.11
FeO	5.85	9.79	9.21	5.80	2.67	1.78	8.77	3.63	2.45	11.06	11.20	11.51
MgO	4.23	6.42	2.64	0.75	0.54	0.30	6.94	0.57	0.13	6.04	5.53	5.34
MnO	0.08	0.21	0.23	0.13	0.10	0.06	0.12	0.22	0.21	0.24	0.18	0.23
CaO	13.40	11.18	6.78	3.87	2.46	1.66	11.95	2.81	1.76	10.77	10.25	10.08
Na ₂ O	1.96	1.92	2.87	2.69	2.88	2.54	1.91	2.57	2.28	1.86	2.16	2.06
K ₂ O	0.19	0.33	0.32	0.39	1.29	1.86	0.29	0.98	1.23	0.35	0.40	0.39
Total	97.79	97.00	96.71	96.60	94.83	93.40	97.23	94.52	93.93	96.76	97.17	97.63
Hole	838A											
Core	9	11										
Type	H											
Section	3	6										
Top	9	39										
Bottom	12	41										
Measuring point	104	33	14	18	24	22						
Depth (mbsf)	75.45	97.92										
Age (ka)	1798	1921										
SiO ₂	54.34	50.35	53.35	57.84	60.13	69.90						
TiO ₂	1.24	0.91	1.22	1.09	0.98	0.79						
Al ₂ O ₃	14.03	16.05	13.18	14.45	14.51	12.47						
FeO	11.24	11.93	14.02	10.54	9.92	5.20						
MgO	3.58	5.07	4.43	2.70	2.63	1.00						
MnO	0.11	0.20	0.23	0.17	0.28	0.20						
CaO	8.08	11.77	9.12	7.54	7.47	4.14						
Na ₂ O	2.51	2.05	2.11	2.13	2.37	0.44						
K ₂ O	0.72	0.16	0.26	0.30	0.24	0.25						
Total	95.85	98.49	97.92	96.76	98.53	94.39						

Ages discussed in this study were estimated from the interpolation of sediment accumulation rate curves (Parson, Hawkins, Allen, et al., 1992) determined using the time scale of Berggren et al. (1985). These interpolated ages have to be treated with utmost caution and are used as relative age indicators in individual drill sites. They are not valid for cross-correlation because present linear interpolation neglects the almost instantaneous deposition of volcaniclastic units several tens of meters thick (especially in Sites 837, 838, and 839). Moreover, locations of biostratigraphic events considered for calculation of sedimentation rates have been frequently found in critical positions (e.g., in the center of thick volcaniclastic deposits and in slump deposits).

DESCRIPTION OF VOLCANICLASTIC DEPOSITS

In the following, volcaniclastic deposits from Sites 834 and 835 are described and discussed in one section according to types of deposits and their respective ages. Sites 836, 837, 838, and 839 are described and discussed individually in stratigraphic order.

“Old Crust” Sites (834 and 835)

Sites 834 and 835, only 48 km apart, were drilled proximal to the Lau Ridge (remnant arc) into “old” backarc basin crust of >4.2 and 3.4 m.y., respectively. Forty beds, rich in vitric shards, ranging in thickness from <1 to 185 cm, and almost all of epiclastic origin, were distinguished in Site 834, mostly restricted to the time span before 2.4 Ma. Volcaniclastic input into Site 835, mostly older than 2.8 Ma, was considerably lower, with some 20 beds not exceeding 37 cm in thickness and mostly <20 cm thick. The paucity of volcaniclastic input into this site is most likely directly related to its sheltered position in a deep, fault-bounded, north-south elongated basin (Fig. 2).

High-K Calc-alkaline Subaerial Fallout Tephra

Three fallout tephra in Samples 135-834A-5H-5, 78 cm (4 cm thick, $Md_{\phi} = 4.77 \Phi$, 2.35 Ma), 135-834A-7H-5, 103 cm (11 cm thick, 3.1 Ma), and 135-834A-7H-5, 148 cm (7 cm thick, 3.15 Ma) occur as discrete, weakly graded beds with sharp upper and lower boundaries within clayey nannofossil ooze. All three are hornblende and/or biotite-bearing, high-K calc-alkaline, high-silica rhyolites (glass composition: 75.7–80.3 wt% SiO₂) with almost identical chemical compositions (Figs. 3–7) and bulk-rock Ba/Zr ratios of 3.8 to 4.5. Volcanic glasses differ compositionally from all other high-silica rhyolites drilled in the Leg 135 Lau Basin sites (see below), by their higher K₂O (3.5–4.5 wt%) and Al₂O₃ (12.8–14.8 wt%), and lower TiO₂ (0.06–0.22 wt%), FeO^o (0.64–1.24 wt%), MgO (0.08–0.39 wt%), CaO (0.28–1.13 wt%), and FeO^o/MgO ratio (2.8–9.2).

Rocks from the Tavua caldera in north central Viti Levu (Fiji), including biotite-bearing shoshonites, have K-Ar ages ranging from 2.48 ± 0.48 Ma to 5.18 ± 10 Ma (Whelan et al., 1985) partially overlapping with the ages of the fallout layers. These shoshonites, however, have as much as 7.5 wt% K₂O at 60 wt% SiO₂ (Gill, 1970) as well as high Ba/Zr ratios around 10. Thus, the compositions found in Hole 834A would require additional fractionation of K-feldspar, a phase not found either in the ODP samples or on Viti Levu. It is not likely that the Tavua caldera was the eruptive site for the high-K, calc-alkaline fallout tephra.

Another potential source is the Tauranga Arc, which was active on North Island (New Zealand) 3.0–0.75 m.y. ago (Smith et al., 1977), though farther away from the Lau Basin (about 1600 km). North Island is notorious for explosive eruptions of high silica rhyolites during the Pleistocene, producing widespread ash layers very similar in composition to the three fallout ashes in Hole 834A (e.g., Kyle and Seward, 1984; Shane and Frogatt, 1991). The striking chemical similarity of all three ashes erupted over a time interval of >0.6 m.y. is a strong argument for their origin from New Zealand. The lack of pronounced chemical variations in rhyolites, interpreted to have resulted from the partial fusion of large volumes of Mesozoic graywacke-argillite sediments (Ewart and Stipp, 1968; Ewart et al., 1977) is a problem in the Cenozoic tephrostratigraphy of New Zealand.

Epiclastic Deposits and Submarine Tephra

>3.3 Ma

Early Pliocene volcaniclastic deposits in the time span between 3.8 and 3.3 Ma were only recorded at Site 834. Bulk rocks are basaltic andesite to rhyolite, with characteristic high Ba/Zr ratios ranging from 5.4 to 6.2 (Fig. 6). The oldest sample (135-834A-16X-2, 9–11 cm) is

Table 3. Representative selected chemical analyses of volcanoclastic bulk rocks by X-ray and infrared spectrometry from Sites 834–839.

Hole:	834A	834A	834A	834A	834A	834A	834A	835A	835A	836A	836A	836A
Core, Section:	5H-5	6H-8	7H-4	7H-5	8H-4	9H-6	16X-2	5H-6	15H-6	2H-4	2H-6	3H-3
Interval (cm):	76-78	33-35	64-65	101-78	33-35	101-103	9-11	73-76	71-73	91-93	39-41	68-70
Depth (mbsf):	42.85	55.00	60.29	62.15	69.43	82.69	132.71	47.21	141.01	6.64	9.10	14.69
Age (ka):	2350	2850	3050	3100	3300	3600	3800	650	3120	261	361	529
Major elements (wt%)												
SiO ₂	56.29	67.00	60.34	65.41	39.19	67.27	56.85	57.67	68.45	50.35	55.00	53.98
TiO ₂	0.35	0.64	0.61	0.29	0.87	0.48	0.62	0.58	0.37	0.56	0.74	1.30
Al ₂ O ₃	13.95	11.87	11.95	15.43	15.04	12.16	16.67	14.71	12.25	12.15	15.08	14.58
FeO	3.21	5.04	5.33	2.39	7.05	3.27	6.24	8.04	4.71	9.43	9.71	11.97
MnO	0.39	0.15	0.12	0.12	0.16	0.20	0.26	0.16	0.13	0.24	0.17	0.19
MgO	1.61	0.93	1.60	1.35	2.81	0.62	2.35	2.88	0.40	2.96	4.05	3.88
CaO	9.26	4.41	7.41	3.33	19.89	4.09	8.45	8.82	2.89	14.86	9.56	8.20
Na ₂ O	3.43	3.46	2.57	3.48	1.72	4.00	3.29	2.45	4.18	1.62	1.99	2.70
K ₂ O	2.37	0.47	0.56	2.85	1.01	1.18	0.40	0.75	1.38	0.43	0.64	0.25
P ₂ O ₅	0.17	0.13	0.12	0.16	0.19	0.09	0.09	0.10	0.07	0.09	0.11	0.12
SO ₃	n.d.	0.03	0.03	0.01	0.03	0.01	0.63	0.01	n.d.	0.02	0.01	0.04
H ₂ O ⁺	2.53	3.78	4.95	3.24	1.17	4.33	1.76	1.42	4.10	0.8	1.01	1.57
CO ₂	4.96	0.58	3.05	0.33	8.97	1.39	0.38	1.55	0.26	6.20	0.94	0.36
Total	98.52	98.49	98.64	98.39	98.09	99.09	98.00	99.15	99.19	99.71	99.00	99.13
Trace elements (ppm)												
S	120	180	320	30	130	120	17030	140	n.d.	250	120	340
Sc	7	23	21	11	20	16	25	31	14	39	32	33
V	91	36	114	50	308	43	144	231	11	325	346	415
Cr	18	11	15	14	45	7	23	14	14	10	32	25
Co	7	1	6	n.d.	17	2	29	n.d.	4	24	18	1
Ni	37	5	18	11	14	2	17	11	3	16	24	22
Cu	42	15	83	44	110	16	108	95	n.d.	142	95	103
Zn	443	171	815	157	133	137	472	240	140	202	177	104
Ga	17	12	11	14	18	13	20	11	19	15	14	14
Rb	32	5	7	46	20	14	4	13	22	5	8	7
Sr	982	182	281	523	634	183	358	270	105	323	274	150
Y	15	37	36	11	16	45	26	19	67	17	22	31
Zr	113	66	77	139	45	107	60	48	169	25	38	59
Ba	504	218	254	531	186	581	361	154	147	136	143	56
Nd	24	18	13	22	15	20	17	14	19	17	6	11
Hole: 838A 839A												
Core, Section:	4H-3	4H-3	4H-3	5H-3	5H-7	7H-6	8H-6	9H-2	9H-3	11H-6	11H-6	1H-3
Top:	100-102	100-102	59-61	88-90	40-42	46-48	74-76	139-142	9-12	39-41	39-41	30-32
Depth (mbsf):	26.77	26.77	29.42	38.09	41.82	63.62	68.94	75.45	75.45	97.92	97.92	3.30
Age (ka):	856	856	933	1186	1295	1732	1762	1798	1798	1921	1921	366
Major elements (wt%)												
SiO ₂	54.26	49.81	52.31	58.59	63.33	69.94	70.42	50.96	51.55	61.88	58.02	51.78
TiO ₂	0.53	0.96	0.86	1.07	0.97	0.51	0.29	0.70	0.77	0.80	0.89	0.59
Al ₂ O ₃	18.28	15.16	14.80	14.93	13.27	12.38	11.92	18.69	17.10	13.41	14.80	15.18
FeO	6.52	11.50	8.83	8.69	6.16	2.64	2.72	8.90	9.84	7.36	9.02	9.18
MnO	0.18	0.27	0.18	0.20	0.16	0.18	0.66	0.18	0.23	0.18	0.18	0.49
MgO	3.97	5.65	3.71	3.30	1.55	0.66	0.33	5.11	5.63	2.32	3.25	4.27
CaO	10.74	10.39	11.35	7.37	5.19	2.59	2.40	11.92	11.20	5.48	7.20	10.79
Na ₂ O	2.14	1.72	2.29	2.81	3.42	3.97	3.89	1.67	1.75	3.05	2.64	1.57
K ₂ O	0.36	0.27	0.62	0.85	1.19	1.53	1.46	0.28	0.30	0.46	0.36	0.39
P ₂ O ₅	0.11	0.17	0.14	0.22	0.24	0.07	0.03	0.06	0.07	0.10	0.09	0.10
SO ₃	0.01	0.03	0.04	0.04	0.01	0.01	n.d.	0.01	n.d.	0.01	0.02	0.01
H ₂ O ⁺	1.41	1.14	1.36	1.88	3.03	3.55	3.76	0.91	0.96	3.04	2.32	2.41
CO ₂	0.71	1.28	2.92	0.08	0.49	0.13	0.18	0.06	0.07	0.07	0.07	1.92
Total	99.22	98.35	99.41	100.03	99.01	98.15	98.06	99.45	99.47	98.16	98.85	98.68
Trace elements (ppm)												
S	50	160	270	290	110	210	10	110	80	170	190	300
Sc	27	37	32	34	18	14	13	36	45	22	33	40
V	155	285	269	221	90	32	12	306	335	142	231	319
Cr	76	64	25	12	9	9	5	23	31	12	14	54
Co	11	23	27	13	13	9	n.d.	20	26	22	26	19
Ni	22	14	17	11	7	4	12	23	35	8	12	42
Cu	20	21	76	83	12	2	n.d.	120	103	40	86	119
Zn	102	159	155	135	157	88	165	135	99	136	142	573
Ga	18	16	17	18	18	15	14	17	18	17	18	14
Rb	5	5	9	17	19	22	20	4	3	3	5	5
Sr	262	235	293	230	228	158	181	212	205	168	174	245
Y	18	16	24	35	41	44	46	17	18	35	25	19
Zr	28	22	52	72	98	131	107	25	29	61	46	19
Ba	158	139	156	182	252	263	280	53	67	143	121	206
Nd	5	1	21	12	29	21	16	6	12	2	12	3

a polymict mixture, mostly of abundant crystals including clinopyroxene, hypersthene, plagioclase, biotite, opaques, quartz, and lithic fragments. Vitric shards are almost pervasively altered to palagonite and dark brown clay minerals.

Sample 135-834A-9H-6, 101–103 cm (82.69 mbsf; 3.6 Ma), from the lower of two well-sorted, upward-fining volcanoclastic units, 57 and 170 cm thick, light to dark gray and thickly to thinly laminated with a Md_{ϕ} of 3.8 Φ (72 μ m) close to the base, is characterized by variable shard morphologies, most of which are very delicate and often have extremely high aspect ratios (Fig. 8). These are low-K rhyolite with small chemical variations of 72.3–76.8 wt% SiO₂ and 1.0 to 1.2 wt% K₂O (Table 2).

Glass compositions follow the major trend (low-K series, LKS) of recent Lau Basin basement lavas (Fig. 4) (Sunkel, 1990; G. Sunkel, unpubl. data). Judging from the chemical homogeneity of the shards, we relate the origin of this unit to a single eruption. As in-situ volcanic rocks with similar chemical compositions are not known from the margins or within the Lau Basin, we can only speculate about the location of this source. The very delicate shapes of the shards, and the relative thickness and massiveness of the deposit suggest little or no reworking. We favor a deep submarine origin for the volcanoclastic units in Sections 135-834A-9H-5 and -9H-6 in spite of the high Ba/Zr ratios.

Table 3 (continued).

Hole:	836A	837A	837A	837A	837A	838A						
Core, Section:	3H-3	1H-5	3H-1	3	4H-2	5H-5	6H-5	7H-2	8H-1	8H-4	9H-3	3H-2
Interval (cm):	68-70	84-86	89-91	32-34	122-124	17-19	22-24	140-142	56-58	113-115	44-46	141-143
Depth (mbsf):	14.69	6.86	18.52	20.82	29.72	52.28	52.28	57.92	67.05	70.66	77.97	16.30
Age (ka):	529	343	568	587	1459	1605	1605	1654	1732	1825	2059	583
Major elements (wt%)												
SiO ₂	54.21	70.68	57.79	67.99	68.06	67.97	55.34	70.05	52.73	57.16	53.74	49.90
TiO ₂	1.29	0.42	0.4	0.42	0.45	0.45	0.47	0.44	0.61	0.87	0.82	0.47
Al ₂ O ₃	14.62	11.61	10.90	12.08	11.88	11.89	12.96	11.95	14.31	15.08	15.50	10.50
FeO	11.78	3.68	3.50	4.03	3.26	3.25	4.24	2.34	5.26	7.99	10.25	4.14
MnO	0.20	0.15	0.10	0.21	0.15	0.15	0.12	0.19	0.22	0.18	0.38	0.14
MgO	3.88	0.80	1.03	0.82	1.08	0.97	1.84	0.49	2.91	2.82	5.02	1.40
CaO	8.27	3.91	11.95	4.10	4.26	4.09	12.32	2.95	12.75	8.25	9.83	16.43
Na ₂ O	2.76	3.03	2.82	3.22	3.15	3.18	2.40	3.94	2.64	2.68	1.81	2.45
K ₂ O	0.25	1.01	0.62	0.89	1.04	1.03	0.63	1.36	0.66	0.41	0.36	0.55
P ₂ O ₅	0.11	0.10	0.07	0.07	0.08	0.08	0.08	0.07	0.11	0.10	0.09	0.08
SO ₃	0.05	n.d.	0.01	n.d.	n.d.	0.01	n.d.	n.d.	0.01	0.03	0.01	0.01
H ₂ O ⁺	1.20	3.29	2.91	4.07	4.14	4.07	2.52	4.19	1.76	1.93	1.40	2.49
CO ₂	0.09	0.47	6.82	0.74	1.07	0.90	5.71	0.6	4.99	1.05	0.21	10.1
Total	98.71	99.15	98.92	98.64	98.62	98.04	98.67	98.57	98.97	98.55	99.42	98.66
Trace elements (ppm)												
S	300	60	140	100	100	360	500	30	150	150	220	140
Sc	32	20	20	14	21	14	21	13	24	28	36	15
V	420	39	66	41	54	49	123	18	147	227	355	92
Cr	11	11	9	11	9	16	31	5	42	14	15	13
Co	21	n.d.	28	4	n.d.	n.d.	13	15	20	9	26	10
Ni	14	10	3	13	7	5	22	11	20	10	34	12
Cu	99	34	32	45	13	21	24	n.d.	37	49	97	41
Zn	119	332	217	343	293	358	172	118	131	254	140	149
Ga	21	10	13	10	9	9	12	12	16	15	18	9
Rb	0	14	5	11	11	13	8	22	9	2	6	6
Sr	147	183	290	145	177	168	307	165	342	182	187	387
Y	32	27	29	34	30	32	23	47	27	31	22	25
Zr	57	49	57	79	71	72	54	124	65	47	29	57
Ba	52	297	263	337	273	286	188	267	156	140	82	188
Nd	20	11	16	11	10	18	15	28	19	12	6	8
Hole: 839A												
Core, Section:	2H-1	3H-6	4H-4	5H-3	6H-6	7H-6	9H-2	10H-4	21X-CC			
Interval (cm):	39-41	140-142	110-112	129-131	42	129-131	129-131	102-104	36			
Depth (mbsf):	4.89	22.9	29.1	37.29	50.42	60.79	73.79	86.02	186.56			
Age (ka):	502	754	754	1031	1618	1685	1714	1714	1828			
Major elements (wt%)												
SiO ₂	66.44	71.72	65.81	54.78	69.10	64.89	67.45	58.89	53.40			
TiO ₂	0.40	0.33	0.45	1.39	0.46	0.53	0.46	0.49	0.65			
Al ₂ O ₃	11.14	11.60	12.70	14.47	12.30	13.47	12.49	17.16	15.80			
FeO	3.93	2.72	3.98	10.53	3.09	4.19	3.40	5.07	9.50			
MnO	0.35	0.09	0.11	0.20	0.10	0.12	0.11	0.37	0.17			
MgO	0.91	0.48	1.01	3.32	0.84	1.46	1.09	2.75	5.45			
CaO	5.75	2.98	5.81	7.78	4.25	6.15	5.04	8.56	10.48			
Na ₂ O	2.74	3.52	3.20	3.18	3.36	2.96	3.20	2.51	1.55			
K ₂ O	0.96	0.88	0.72	0.46	0.97	0.82	0.90	0.55	0.36			
P ₂ O ₅	0.11	0.04	0.06	0.20	0.09	0.13	0.11	0.07	0.06			
SO ₃	n.d.	n.d.	0.01	0.07	n.d.	0.03	0.01	0.01	0.04			
H ₂ O ⁺	3.49	3.8	3.25	1.63	3.58	3.11	3.47	2.17	1.58			
CO ₂	1.99	0.36	1.42	0.59	0.73	1.17	1.04	0.18	0.21			
Total	98.21	98.52	98.62	98.6	98.87	99.03	98.77	98.78	99.25			
Trace elements (ppm)												
S	170	10	100	470	60	810	350	140	540			
Sc	25	15	15	28	14	23	16	25	35			
V	50	26	77	339	50	99	62	123	301			
Cr	6	5	8	5	23	24	16	59	57			
Co	n.d.	11	1	21	10	n.d.	1	19	10			
Ni	11	2	0	10	9	5	1	20	30			
Cu	30	0	17	42	8	17	4	66	114			
Zn	609	213	120	145	144	112	133	106	207			
Ga	8	10	9	17	11	11	10	16	15			
Rb	12	9	9	7	11	10	13	5	6			
Sr	261	120	162	190	158	189	175	222	187			
Y	31	34	31	38	30	31	30	23	18			
Zr	54	69	62	79	71	63	69	43	25			
Ba	326	318	253	77	257	227	254	146	129			
Nd	8	6	15	14	22	17	14	9	10			

3.3 Ma

One epiclastic unit, 135 cm thick, was distinguished at 69.50 mbsf of Hole 834A (Parson, Hawkins, Allan, et al., 1992), differing from all other volcanoclastics in Sites 834 and 835 in composition and by sedimentologic criteria. It is made up of numerous, alternating light to medium gray and dark gray to black layers, dominantly silt-sized and overall fining upward, but locally reaching grain sizes of up to 1 mm. The major components are varying proportions of medium brown, highly scoriaceous shards with incipient palagonitization (Fig. 9), igneous minerals, and neritic foraminifers. Two samples of about 3.3 Ma (135-834A-8H-3, 118–120 cm, and 135-834A-8H-4, 33–35 cm) with a Md_{Φ} of 2.13 Φ (0.23 mm) and 3.20

Φ (0.11 mm), respectively, were studied in detail. They represent the coarsest volcanoclastics recovered from Sites 834 and 835. Plagioclase dominates the phenocrysts, followed by hypersthene, hornblende, biotite, and opaques. Volcanic glasses and bulk rocks are calc-alkaline basaltic, with SiO₂ averaging around 51.4 wt% and K₂O around 1.8 wt% (Fig. 4). The glasses are also characterized by high TiO₂ (averaging around 1.7 wt%), CaO (mean 9.3 wt%) and MgO (mean 4.4 wt%) (Fig. 3). Shards from these two samples, which extend into the basaltic andesite/andesite range, are characterized by extreme K₂O-enrichment (3.0 wt% at 54.3 wt% SiO₂), slightly extending into the shoshonitic field (Table 2).

This unit correlates stratigraphically and compositionally very well with subaerial volcanics on the neighboring Lau Ridge islands,

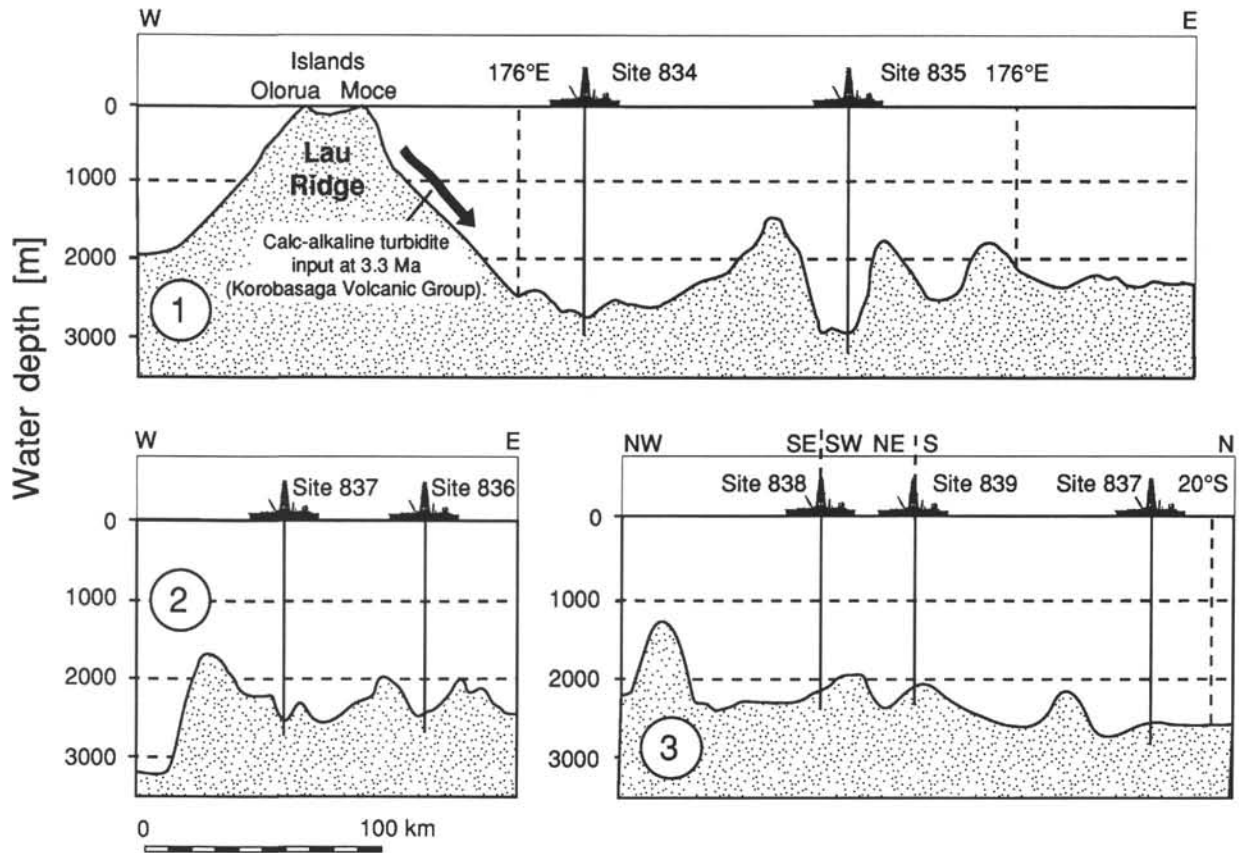


Figure 2. Bathymetric cross-sections of the Lau Basin, showing the positions of Sites 834 through 839. For the position of Profiles 1, 2, and 3, see Figure 1. Bathymetric data from Parson et al. (1992).

Moce and Olorua. They belong to the Korobasaga Volcanic Group, with estimated ages between 2.5 and 4.5 Ma (Cole et al., 1985). Note that the bulk analyses agree also with the lower TiO_2 and Al_2O_3 concentrations of the Moce and Olorua basalts. Rare basaltic andesitic and andesitic shards with increased K concentrations are geochemically similar to the Lau Volcanic Group (>6 Ma) on Ono-I-Lau Island, >200 km to the south. We do not expect direct input from this old material from Ono-I-Lau Island into Site 834. It is more likely that during the time of Korobasaga volcanism, rare high-K andesites evolved and erupted occasionally, but that they are no longer exposed on any of the Lau Islands.

We interpret the two volcanoclastic units in sections 135-834A-8H-3 and -8H-4 to have been deposited by turbidity currents directly related to the eruption and deposition of tephra from explosive volcanism on Moce and Olura islands on the Lau Ridge. A subaerial to very shallow submarine (<200 m water depth) origin for the tephra is strongly suggested by the high vesicularity of the basaltic clasts (Fig. 9) and the occurrence of neritic foraminifers unique in all of Sites 834 and 835.

<3.3 Ma

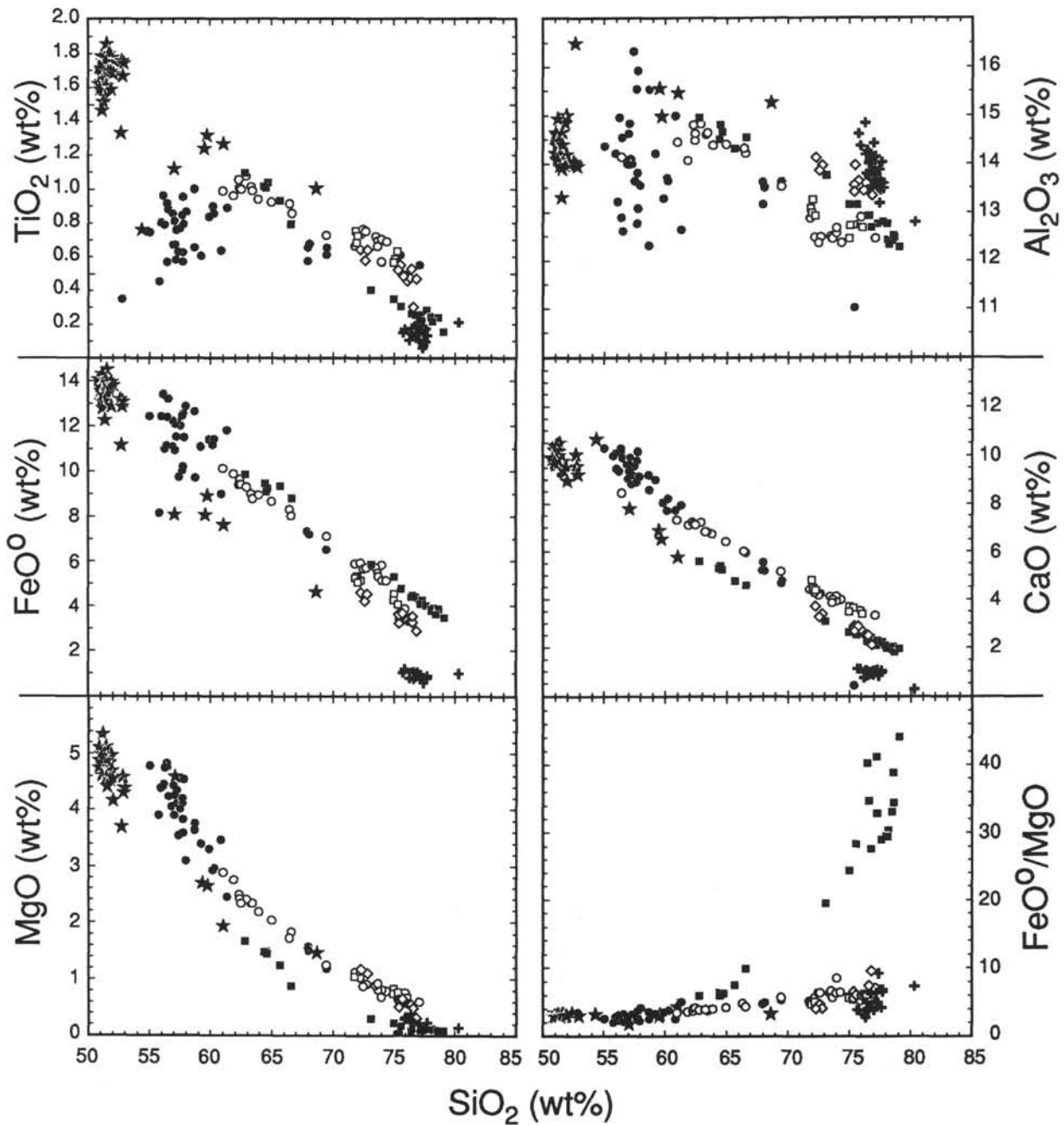
Three magmatic groups are distinguished in the non-calc-alkaline volcanoclastic rocks of Sites 834 and 835 <3.3 Ma (Figs. 3–5).

1. Sample 135-835A-15H-6, 71–73 cm (141.01 mbsf, 3.1 Ma) is from a coarse-grained ($Md_\phi = 2.38 \Phi$, 0.19 mm), ungraded and structureless gray volcanoclastic layer, 23 cm thick, with sharp contacts to underlying and overlying, very dark brown nanofossil ooze. Colorless to very light brown pumice clasts of low to medium vesicularity, often with tubular vesicles, make up most of the sedi-

ment. Many shards have very delicate, curved to sharply bent morphologies, or very thin spikes and needles with extreme aspect ratios. Medium brown shards and colorless bubble junction shards are rare. Single crystals are almost absent.

Glasses are dacitic to rhyolitic and correspond to the low-K series trend (LKS) of the Lau Basin basement (Fig. 4) with a compositional gap between 67 and 73 wt% SiO_2 . The concentrations and evolution of other elements, however, differ when compared with other samples following the LKS trend (Fig. 5), including a steeper gradient of TiO_2 during differentiation, slightly higher FeO° concentrations, and distinctly lower CaO and MgO concentrations. Less effective FeO° decrease and low MgO concentrations result in a rapid increase of the $\text{FeO}^\circ/\text{MgO}$ ratio in the rhyolites, which is unique in all samples from Sites 834 and 835 (Fig. 5). The Ba/Zr ratio of 0.87 is similar to that from Lau Basin basement lavas (Fig. 6), but it is distinctly lower than all other samples from Sites 834 and 835.

A unique and well-defined geochemical trend of the volcanoclastic layer at 141.01 mbsf of Hole 835A is taken as unequivocal evidence for its origin from a single eruption. The observed chemical variation suggests the existence of a zoned magma chamber before eruption. The general appearance, homogeneity, delicate shapes of particles, lack of grain-size grading, and good sorting of this layer, interbedded with nanofossil ooze, suggests an origin as subaerial fallout ash. We favor, however, the origin from a submarine eruption because of the great similarity of geochemical trends with the magmatic evolution of the Lau Basin basement. This sample has the lowest Ba/Zr ratios of all Lau Basin rhyolites analyzed for this study (i.e., it is closest to most of the Lau Basin basement lavas). Furthermore, no evidence is present that the modern Tofua Arc already existed at that time (Hawkins et al., 1984; J. Gill, pers. comm., 1992). Tonga Ridge volcanism has a different composition during that period. It is also striking that the elongate to



Hole 834A:

- + 5H-5, 76-78 cm (42.85 mbsf, 2.4 Ma); 7H-5, 101-103 cm (62.15 mbsf, 3.1 Ma); 7H-5, 147-148 cm (62.57 mbsf, 3.2 Ma) (high-K calc-alkaline fallout tephra)
- 6H-2, 36-37 cm (47.45 mbsf, 2.7 Ma); 6H-7, 33-36 cm (55.00 mbsf, 2.8 Ma)
- 7H-4, 64-65 cm (60.29 mbsf, 3.0 Ma)
- ★ 8H-3, 118-120 cm (68.78 mbsf, 3.3 Ma); 8H-4, 33-35 cm (69.43 mbsf, 3.3 Ma) (Lau Ridge Korobasaga Group volcanoclastics from Olorua and Moce islands)
- ◇ 9H-6, 101-103 cm (82.69 mbsf, 3.6 Ma)

Hole 835A:

- 5H-6, 73-76 cm (46.23 mbsf, 0.6 Ma); 5H-7, 16-18 cm (47.21 mbsf, 0.6 Ma)
- 15H-6, 71-73 cm (141.01 mbsf, 3.1 Ma)

Figure 3. Variation diagrams of electron microprobe analyses of vitric shards in samples from Holes 834A and 835A.

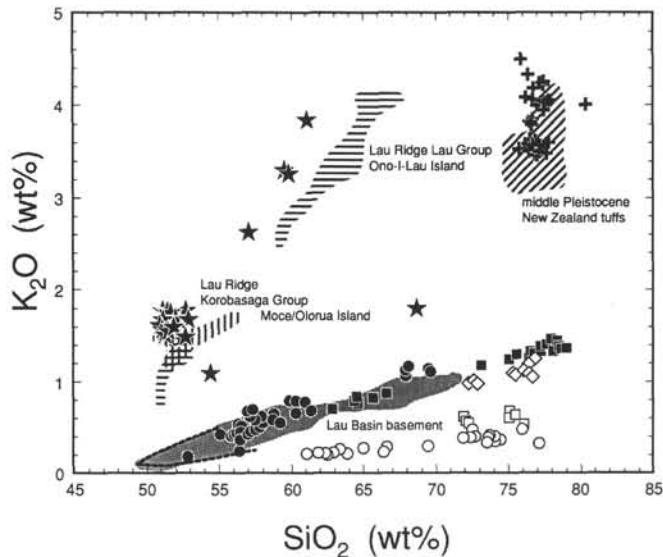


Figure 4. SiO_2 - K_2O variation diagram of electron microprobe analyses of vitric shards in Holes 834A and 835A. Legend as in Figure 3. Reference fields for Lau Ridge volcanics from Cole et al. (1985) and for middle Pleistocene New Zealand tephras from Shane and Frogatt (1991). Dashed lines = differentiation trends of glasses from Lau Basin basement recovered during Leg 135 (Nilsson, this volume).

needle-like shapes and morphologies of vitric shards are very similar to those in sample 135-834A-9H-6, 101–103 cm which has been related to a submarine eruption (see above).

Sample 135-834A-7H-4, 64–65 cm (60.20 mbsf, 3.0 Ma), from a 24-cm-thick laminated volcanoclastic unit, interbedded in nannofossil ooze, is characterized by rhyolitic (71.8–76.0 wt% SiO_2), colorless shards with large external vesicles (Figs. 3–4). Pumiceous clasts, light brownish dense shards, and plagioclase and biotite crystals are rare.

2. Sample 135-834A-6H-7, 33–36 cm (55.00 mbsf, 2.8 Ma) comes from a 65-cm-thick, upward-fining volcanoclastic unit, laminated in the lower 20 cm and grading into nannofossil ooze. It is crystal poor (<1 vol% plagioclase) and dominated by colorless to slightly yellowish bubble wall, bubble junction, platy, and cusped shards with a characteristic high effective vesicularity (former vesicles exceeding the size of the shards). About 30 vol% are made up of angular, tubular vesicle pumice clasts. Medium brown shards with microlites and crystallites are rare. Shards are mostly rhyolitic in composition (71.8–75.9 wt% SiO_2) with rare andesitic and basaltic andesitic glasses (Figs. 3–4).

Sample 135-834A-6H-2, 36–37 cm (47.45 mbsf, 2.7 Ma), was taken from a 2-cm-thick, discrete, graded, vitric ash layer, interbedded between nannofossil ooze. Crystals of plagioclase, hypersthene, clinopyroxene and opaques make up about 10 vol%. Blocky, tubular vesicle shards, and bubble junction, platy, and cusped shards are mostly very light brown with low to medium vesicularity. The glass is andesitic, mostly restricted to the narrow interval between 62.3 and 66.5 wt% SiO_2 , apart from a few rhyolitic shards (Figs. 3–4).

All three samples are very fine-grained ($Md_\phi = 4.6$ – 4.7Φ , ca. 40 μm) and contain varying proportions of alteration products such as Fe-Mn hydroxide micronodules; brownish, greenish, and brownish-greenish clay minerals; and spherulitic aggregates of fibrous zeolites.

These volcanoclastics, representing the time span from approximately 2.7 to 3.0 Ma, are characterized by very low K_2O -enrichment trends (very-low-K series: VLKS). The K_2O concentration at 70 wt% SiO_2 increases slightly from 0.32 wt% to 0.4 and 0.6 wt% upsection. These are well below K_2O concentrations in the LKS, represented for instance by the bulk of the Lau Basin basement (Fig. 4), but lie in the extension of K_2O -enrichment trends for some basement glasses re-

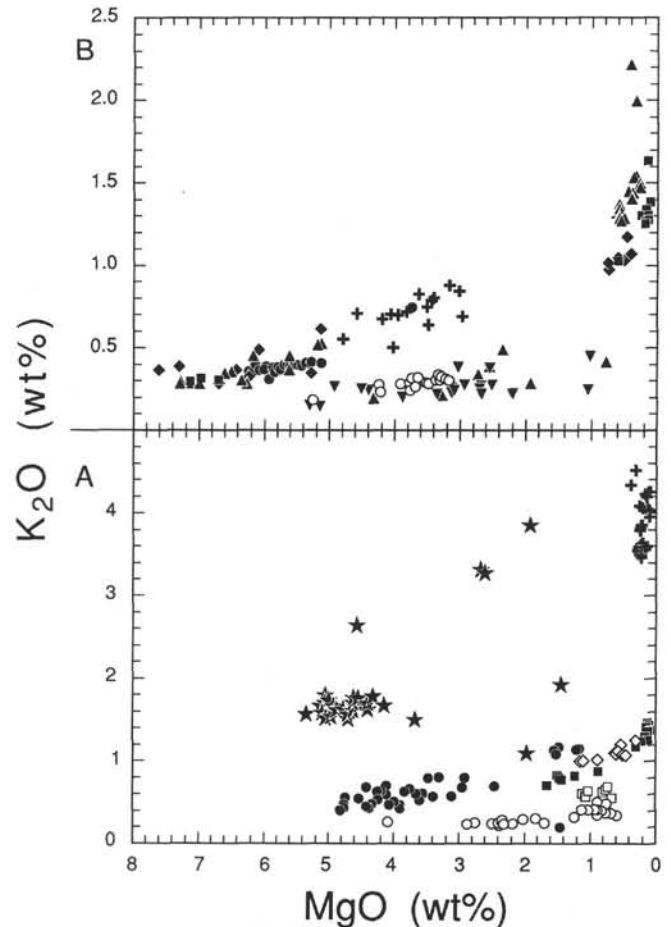


Figure 5. MgO - K_2O variation diagram of electron microprobe analyses of vitric shards. A. Holes 834A and 835A. B. Holes 836A and 838A. Legend as in Figure 3.

covered during Leg 135 (Nilsson, this volume; see thick dashed line in Fig. 4). Basaltic to rhyolitic igneous basement on the island of 'Eua shows similar low K_2O -enrichment trends, but it is of Eocene age (Cunningham and Anscombe, 1985). A (subrecent?) rhyolitic pumice block dredged on the Tonga Ridge has a low K_2O concentration of 0.55 wt% at 71 wt% SiO_2 (Hawkins, 1985), whereas the 1967–1968 eruption of Metis Shoal on the Tonga Ridge produced rhyolitic glass with 1.47 wt% K_2O (Melson et al., 1970), and a Zephyr Shoal dacite has 0.98 wt% K_2O (Hawkins, 1976).

The small grain size of the three samples suggests medial to distal volcanic activity. Unique chemical trends or restricted compositional ranges in each of the units indicate that they are probably the result of individual eruptions. The high effective vesicularity of many shards may indicate subaerial to shallow submarine eruptions. Transport into the site area was by turbidity currents and subaerial fallout (Sample 135-834A-6H-2, 36–37 cm).

We can only speculate about the source as evolved rocks with similar chemical characteristics are not known from any of the potential source areas. It might be derived (1) from eruptions on the Tofua Arc, which was much closer at that time; or (2) from eruptions on a shallow seamount (e.g., Zephyr Shoal, 350 km away from the site to the north, or an unknown seamount).

Judging from the bathymetric fabric of the Lau Basin, which is dominated by north-trending tectonic basins and ridges, Zephyr Shoal is a more likely candidate for the origin, as we can assume turbidite flow along-strike of the tectonic structure of the basin. Furthermore, the Tofua Arc was a nascent arc at the time of deposition.

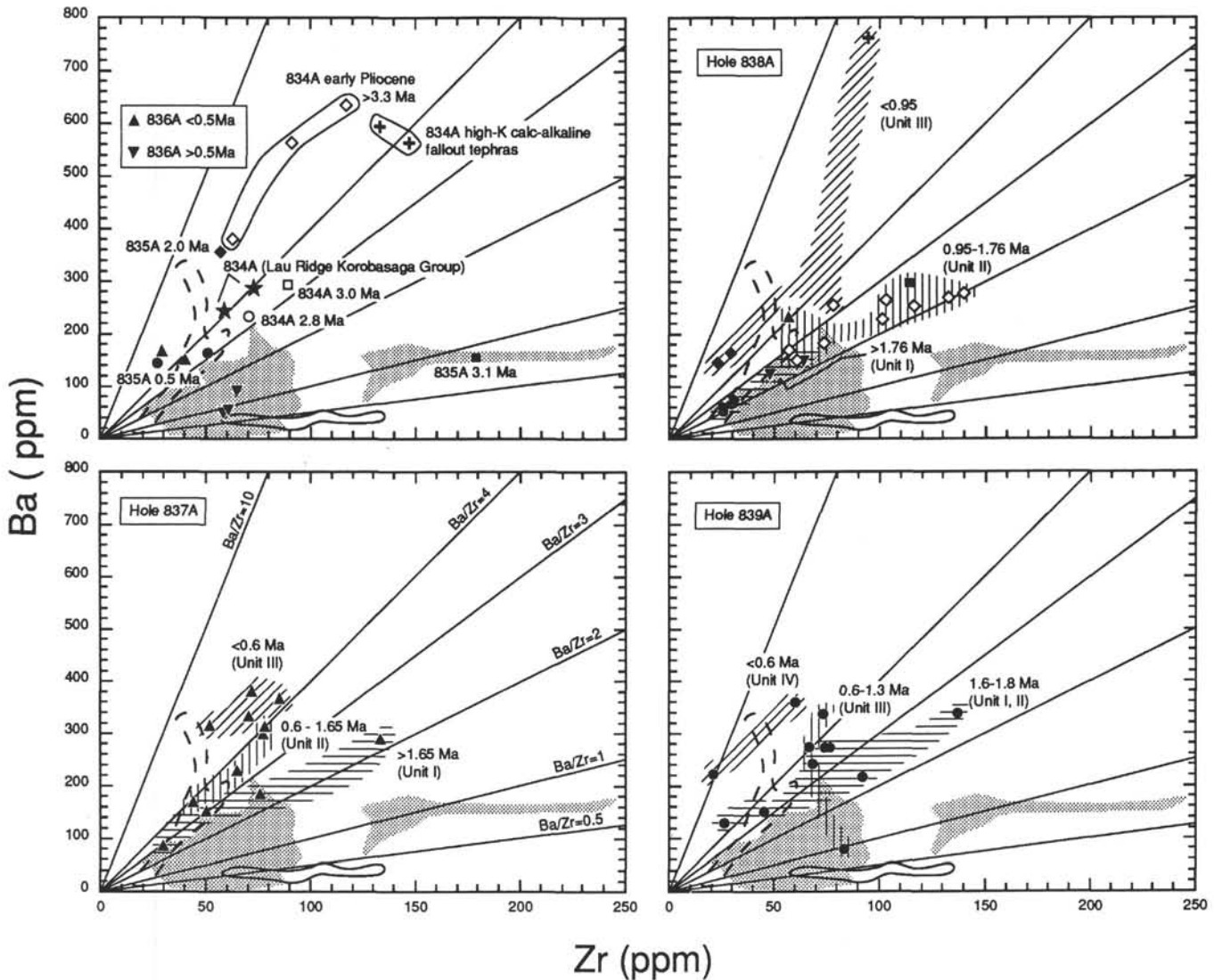


Figure 6. Zr-Ba variation diagrams from X-ray fluorescence (XRF) analyses of volcaniclastic bulk rocks from Holes 834A, 835A, 836A, 837A, 838A, and 839A. Shaded area = Lau Basin basement lavas, including Valu Fa Ridge (Sunkel, 1990; G. Sunkel, unpubl. data). Area marked by dashed line = Metis Shoal Sample USNM 11108 (own analyses), 1935 Fonulai Island (Tonga) eruption (own analyses), and Ata Island (Tonga) (Vallier, O'Connor, et al., 1985). Area marked by solid line = 'Eua Island (Tonga) (Cunningham and Anscombe, 1985).

3. Samples 135-835A-5H-6, 73-76 cm, and -5H-7, 16-18 cm (46.23 and 47.21 mbsf, 0.6 Ma), were taken from two very dark brown, fine-grained ($Md_{\phi} < 4.65 \Phi$; $< 40 \mu\text{m}$) volcaniclastic units, 30 and 15 cm thick, interbedded in brown nannofossil ooze and foraminifer-nannofossil ooze. Both samples are polymictic sediments, made up largely of slightly vesicular, very light to light brownish vitric shards, and less abundant medium to highly vesicular pumice fragments. Dense, blocky, yellowish shards with plagioclase and clinopyroxene microphenocrysts, and broken, angular fragments of plagioclase, clinopyroxene, hypersthene, and few opaques are common. Dark brown, blocky shards are rare. Coarser grained lithic fragments, often with tachylitic groundmass, some with trachytic textures, are more abundant in the older of the two samples. Fragments of green to brown clay minerals, brown fibrous zeolites, and red-brown iron hydroxides occur throughout the samples.

Glasses in both samples are LKS basalts to rhyolites (52.8-75.4 wt% SiO_2) with some large compositional gaps (e.g., 61.3-69.4 wt% SiO_2). Basaltic andesites and low-silica andesites dominate and show considerable scatter, especially with TiO_2 , FeO , and Al_2O_3 (Figs. 3-4). TiO_2 behaves incompatibly below 60 to 62 wt% SiO_2 , rising from 0.35

wt% to maximum concentrations of about 1 wt% when Fe-Ti oxide fractionation begins. Al_2O_3 shows unsystematic variations from 12.1 to 16.3 wt% in the more mafic glasses < 60 wt% SiO_2 and decreases during further differentiation to 11 wt% in the most evolved rhyolite.

We do not relate Samples 135-835A-5H-6, 73-76 cm, and -5H-7, 16-18 cm, directly to specific volcanic eruptions because of the large geochemical and mineralogical heterogeneity, less clearly defined geochemical trends than in many other samples, and a wide range of groundmass textures and abundant secondary minerals, probably indicative of several cycles of reworking. This is in accordance with the small grain size and thickness of the deposit, which also indicates some distance to the source. The abundance of clasts with low to medium vesicularity and common trachytic and tachylitic textures indicate an origin from pillow and sheet lava flows by spalling of glassy rinds and breaking up of flow interiors (e.g., by tectonic activity). Rare pumiceous, highly vesicular fragments of evolved composition suggest minor contributions from subaerial or submarine explosive volcanism. The similarity to the low-K series, largely overlapping with compositions of the Lau Basin basement, is in accordance with an origin from within the Lau Basin.

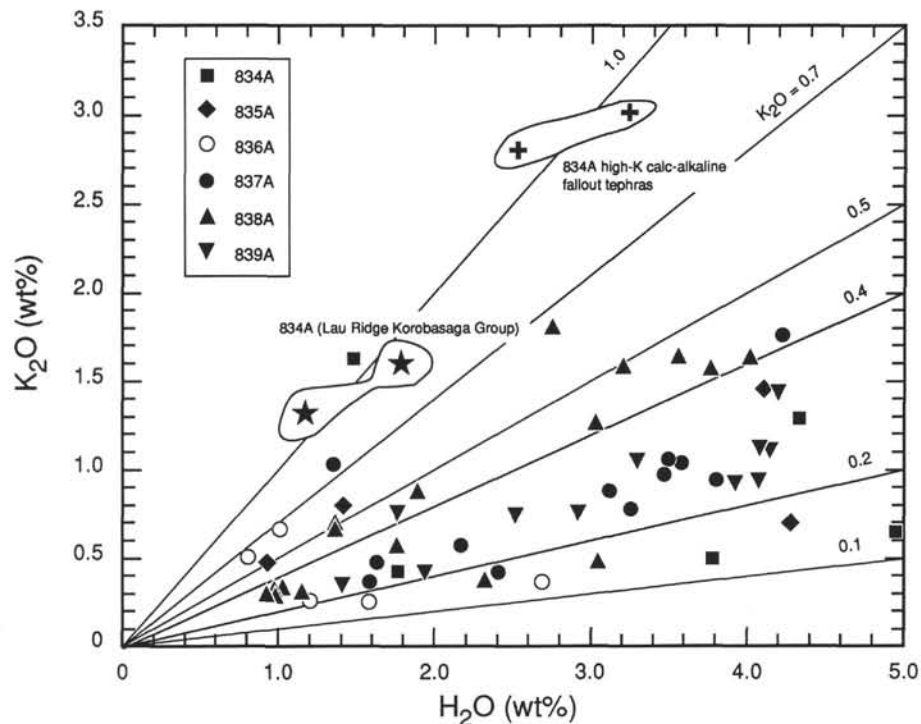


Figure 7. H₂O-K₂O variation diagram from XRF and infrared spectrometry analyses of volcanoclastic bulk rocks from Holes 834A, 835A, 836A, 837A, 838A, and 839A.



Figure 8. Scanning electron microscope (SEM) picture of very delicate, low-K rhyolitic shards, partially with extreme aspect ratios, from Sample 135-834A-9H-6, 101–103 cm (82.69 mbsf), with an age of approximately 3.6 Ma. In spite of a large range in vesicularity and shard morphologies, their chemical composition is rather homogeneous (73–77 wt% SiO₂).

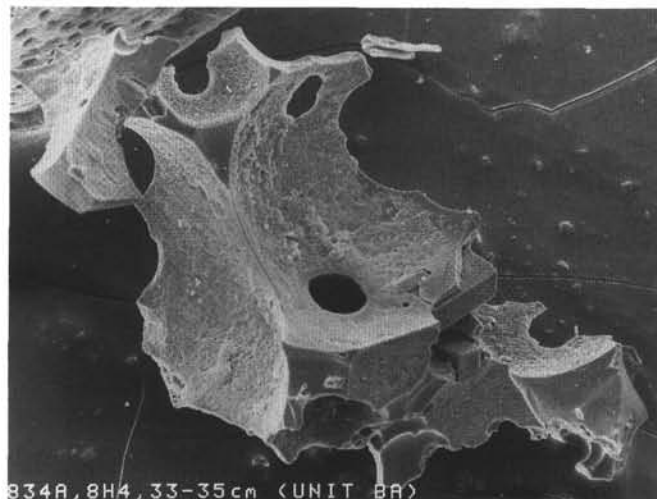


Figure 9. Scanning electron microscope (SEM) picture of highly vesicular, basaltic bubble junction shard from Sample 135-834A-8H-3, 33–35 cm (69.43 mbsf), with an age of 3.3 Ma. It correlates geochemically to the calc-alkaline Korobasaga Volcanic Group (4.5–2.5 Ma) on the Lau Ridge, especially with volcanic rocks found on nearby Moce and Olorua islands (see also Fig. 1).

Central Southern Lau Basin Sites

Site 836

Site 836 is located on the youngest crust of all Lau Basin sites of Leg 135 (about 0.64 Ma). It was drilled into a small basin (about 20 km long and 5 km wide at the 2400 m isobath) about 50 km west of the propagating rift tip of the ELSC in the central Lau Basin (Fig. 1). On the eastern side of the basin, several large seamounts or uplifted

blocks rise to water depths of <1500 m (Parson et al., 1992). Only 20 m of sediments comprise 43 layers rich in volcanoclastics. Mostly blocky and angular grains are often millimeter-sized and reach maximum diameters of up to 2 cm. Individual units range in thickness from 1 to 101 cm, making up about 50% of the lower half of the sedimentary section.

Two magmatic groups are distinguished in the time intervals from 0.6 to 0.5 Ma, and from <0.5 Ma to Holocene by significant differences in the Ba/Zr ratio and sedimentation patterns.

0.6–0.5 Ma (Ba/Zr Ratio 0.9–1.4)

Sample 135-836A-3H-4, 29–31 cm (15.70 mbsf, 0.54 Ma), was taken from a 50-cm-thick, fine-grained volcanoclastic layer ($Md_{\phi} = 3.77 \Phi$, 70 μm). Light brown vitric shards, mostly platy and angular, show a limited compositional range of 54.3 to 58.1 wt% SiO_2 . Igneous minerals are very rare.

Sample 135-836A-3H-3, 68–70 cm (14.69 mbsf, 0.53 Ma) was taken from a coarse-grained ($Md_{\phi} = 0.11 \Phi$, 0.93 mm), graded, black volcanoclastic layer, 91 cm thick. Glasses are basaltic andesites and andesites, ranging from 55.1 to 58.2 wt% SiO_2 . This homogeneous sediment is made up mainly of blocky, angular, light brown clasts and shards of low to medium vesicularity. Many clasts have abundant quench-texture microlites of plagioclase > clinopyroxene, mostly with a trachytic texture. Phenocrysts and microphenocrysts make up <1 vol%.

Five to seven individual layers of basaltic andesitic and andesitic clasts occur per meter of core in the depth interval from 12 to 15 mbsf, corresponding to a depositional rate of 13 layers per 50 k.y. The particles in these layers have formed dominantly from the spalling of glassy pillow rinds and/or the chilled margin of sheet-flow lavas, judging from the predominantly blocky shapes, relative low vesicularity, and abundant trachytic textures of quench microlites. Good sorting and abundant graded bedding indicate redeposition, probably on a local scale. The origin of the hyaloclastites from a proximal source is consistent with large maximum and average grain sizes, angular to subangular shapes of clasts, high sediment accumulation rates, and the high relative abundance of hyaloclastites.

The rapid deposition of hyaloclastites chemically similar to lavas from presently active spreading centers in the Lau Basin (Sunkel, 1990) (Figs. 6 and 10–11) started less than 50 k.y. after the cessation of the effusive volcanic activity that forms the basement at Site 836. Characteristics include the predominance of intermediate rocks not observed in the other volcanoclastics from the Lau Basin. Thus, the hyaloclastites are interpreted to be spreading-related, probably representing spatially discontinuous, late-stage volcanism at the margins of the active volcanic zone of the Eastern Lau Basin Spreading Center, which may have, for instance, built up a small seamount. The bathymetry in the direct vicinity of Site 836 (Fig. 2) shows a seamount rising from water depths of about 2200 to 1500 m less than 5 km to the northeast (Parson et al., 1992).

<0.5 Ma (Ba/Zr Ratio 3.7–5.5)

Sample 135-836A-2H-4, 91–93 cm (6.64 mbsf, 0.26 Ma) derives from a 3-cm-thick layer, is described as “very dark gray coarse vitric ash with foraminifers” ($Md_{\phi} = 3.74 \Phi$, 75 μm), interbedded with brown to dark brown clayey nannofossil ooze. Very light brown shards of mostly low to medium vesicularity and some scoriaceous varieties including abundant igneous minerals (plagioclase, hypersthene, opaques, pigeonite(?), clinopyroxene) have an andesitic bulk composition (59.4 wt% SiO_2). Some rock fragments show zeolite to lower greenschist facies alteration, including (1) a fragment of a quartz vein, (2) an altered fragment with quartz, prehnite, epidote, and FeOOH , (3) a completely altered clast of brown-green clay minerals and fibrous zeolites, and (4) a large clast with quartz, pumpellyite, and chlorite.

Sample 135-836A-2H-6, 39–41 cm (9.10 mbsf, 0.36 Ma) is taken from a “very dark gray medium coarse vitric ash with clay” ($Md_{\phi} = 4.77 \Phi$, 40 μm ; 57.4 wt% SiO_2 , 4.2 wt% MgO , 25 ppm Ni), 5 cm thick, and interbedded in clayey nannofossil ooze. It is a very heterogeneous sediment with mostly dense and low vesicular blocky angular and some more scoriaceous shards (some with trachytic textures). The sediment contains abundant fragments of plagioclase, hypersthene, and opaques as well as a high proportion of strongly altered clasts such as a prehnite-bearing fragment, a thomsonite-natrolite and carbonate-bearing clast, and green-brown to brown clay minerals. Some rock fragments lack intersertal glass in the groundmass, clearly indicating that they are derived from the interior of thick flows, dikes, or sills.

The heterogeneous composition of both volcanoclastic layers, in terms of different groundmass textures, igneous minerals, and abundance of altered clasts and fragments precludes their origin from individual eruptions and suggests several redeposition cycles. The occurrence of lower greenschist facies minerals (e.g., prehnite and pumpellyite) indicates the highest alteration temperatures found in post-lava sediments of the Lau Basin during Leg 135. Their detrital nature is evident from the abundance of fresh glass in the same samples. Altered fragments which may originate from the vicinity of fossil hydrothermal systems and the occurrence of clasts from the interior of flows, sills, or dikes suggest that fault brecciation and subsequent erosion has contributed to the formation of the clasts. Vitric shards, probably of basaltic andesitic to andesitic composition, were most likely originally formed by spalling of glassy flow rinds.

Site 837

Three characteristic units are distinguished using geochemical, petrological, and sedimentological criteria (Fig. 12).

Unit I (Hole 837A)

In Hole 837A, Unit I (55–84 mbsf, 1.7–2.0 Ma) comprises >40 volcanoclastic units with Md_{ϕ} values up to 0.61 Φ (330 μm), ranging in thickness from 2 to 390 cm, but mostly <20 cm thick. Individual units are mostly graded or occur as upward-fining sequences and are vaguely laminated. Interbedded clayey mixed sediments contain abundant dispersed volcanoclastic material.

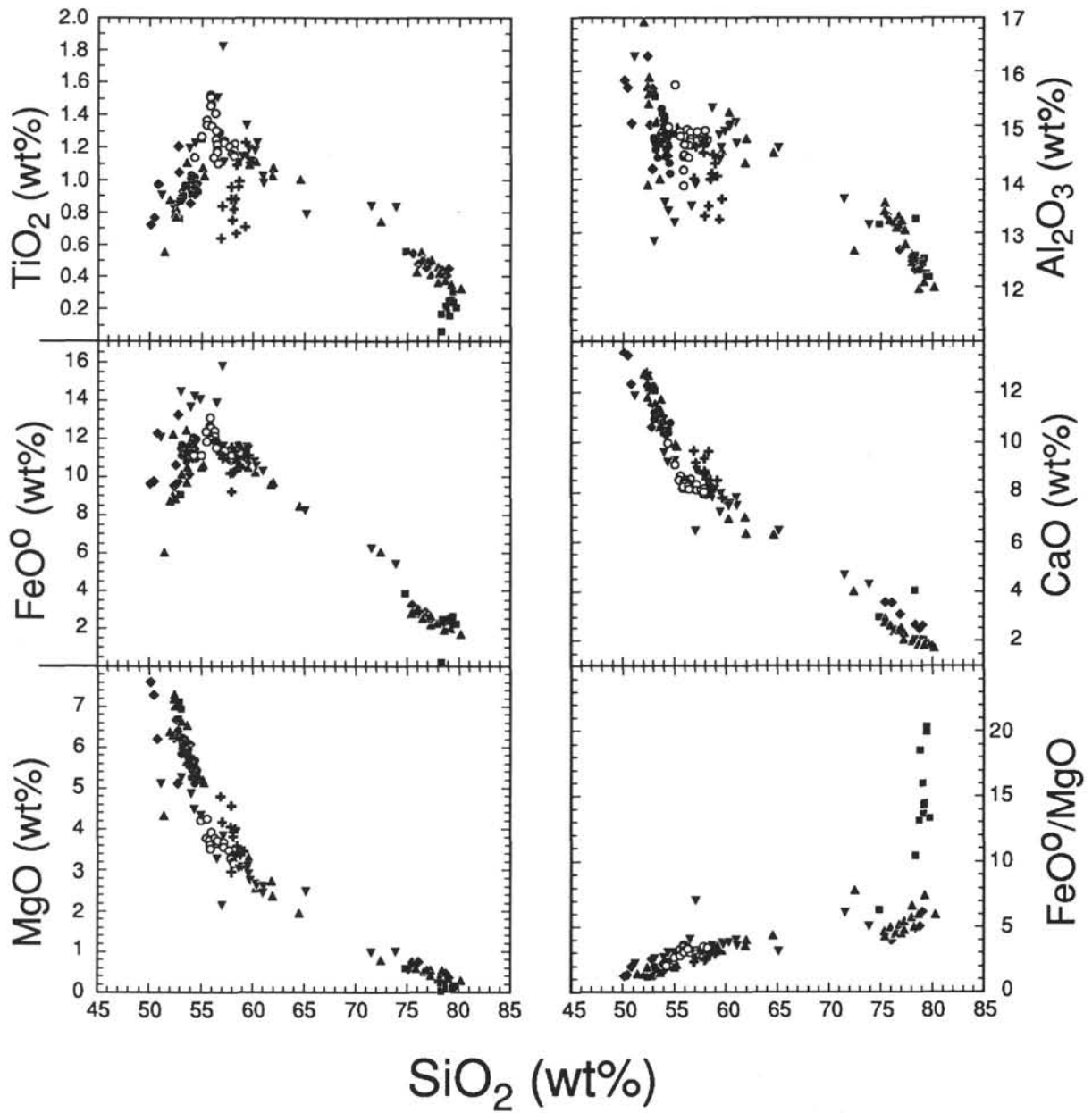
The lower three samples in Unit I (135-837A-9H-3, 44–46 cm [77.97 mbsf, 2.06 Ma]; -8H-4, 113–115 cm [70.66 mbsf, 1.82 Ma] [$Md_{\phi} = 4.62 \Phi$, 41 μm], and -8H-1, 56–58 cm [67.05 mbsf, 1.73 Ma] [$Md_{\phi} = 1.74 \Phi$, 299 μm]) are all heterogeneous and contain significant amounts of mostly pale to dark brown blocky, angular shards of low to medium vesicularity and varying proportions of lithic and tachylitic subangular clasts, often with trachytic textures. Crystals of plagioclase, hypersthene, clinopyroxene and opaques occur throughout. Pale brown to colorless pumiceous shards with higher vesicularity are rare. The bulk chemical composition is intermediate with 55.1–61.4 wt% SiO_2 , 3.0–5.2 wt% MgO , and 0.37–0.77 wt% K_2O . Ba/Zr ratios range from 2.4 to 3.0 (Fig. 6). The contribution of several sources to these deposits is likely because of the lithologic heterogeneity even within individual beds. Spalling of rinds from submarine flows has been the main fragmentation mechanism.

Sample 135-837A-7H-2, 140–142 cm (57.92 mbsf, 1.65 Ma) ($Md_{\phi} = 4.03 \Phi$, 61 μm), is dominated by needle-like colorless shards with relatively high aspect ratios. Colorless bubble wall and bubble junction shards form an important contribution. Different types of pumice clasts occur throughout. Igneous minerals are rare. The rock is a homogeneous rhyolite tephra with 75.3 wt% SiO_2 , 1.46 wt% K_2O , and a Ba/Zr ratio of 2.2 (Fig. 6). This 12-cm-thick, vaguely laminated and graded volcanoclastic bed, interbedded with clayey vitric silt, may be a subaerial fallout layer. A Zr concentration of 133 ppm, much higher than in the other rhyolites of Hole 837A, in which Zr is mostly <80 ppm, is also consistent with a different volcanic source, producing less high-field-strength (HFS) element-depleted lavas.

There is little variation in the Ba/Zr ratios throughout Unit I in Hole 837A, in spite of the compositional heterogeneity of some samples, close to the upper limit of Lau Basin basement rocks (Fig. 6). This seems to imply a single source for the volcanoclastics. Systematically increasing Zr/Y ratios from 1.3 at the base to 2.6 at the top of the unit are in agreement, however, with the assumption of several sources.

Unit II (Hole 837A)

In Hole 837A, Unit II (25–55 mbsf) is dominated by two volcanoclastic layers 17.08 and 8.10 m thick, which are not separated by



Hole 836A:

- 3H-3, 68-70 cm (14.69 mbsf, 0.53 Ma);
- 3H-4, 29-31 cm (15.70 mbsf, 0.54 Ma)

Hole 838A:

- ◆ 2H-3, 147-159 cm (8.18 mbsf, 0.50 Ma) } Unit III
- ◆ 4H-3, 100-102 cm (26.77 mbsf, 0.86 Ma) } Unit III
- ▲ 6H-5, 53-55 cm (50.84 mbsf, 1.56 Ma) } Unit II
- 8H-6, 74-76 cm (68.94 mbsf, 1.76 Ma) } Unit II
- 9H-3, 9-12 cm (75.45 mbsf, 1.80 Ma) } Unit I
- ▼ 11H-6, 39-41 cm (97.92 mbsf, 1.92 Ma) } Unit I

Figure 10. SiO₂-MgO, SiO₂-FeO⁰, SiO₂-TiO₂, SiO₂-FeO⁰/MgO, SiO₂-CaO, and SiO₂-Al₂O₃ variation diagrams of electron microprobe analyses of vitric shards from samples in Holes 836A and 838A.

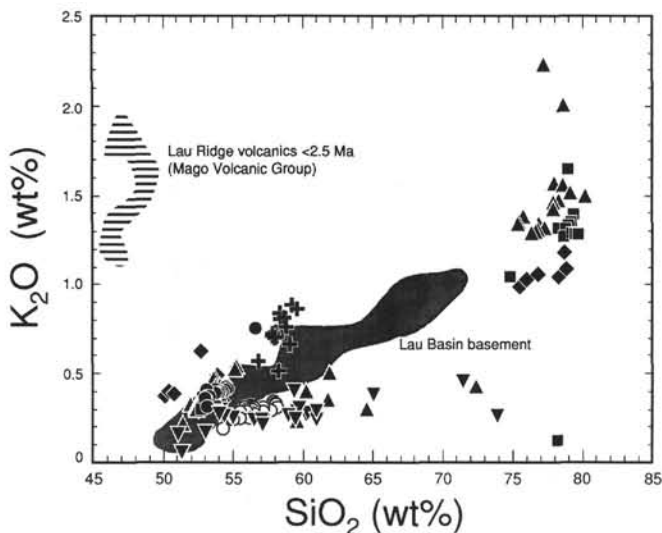


Figure 11. SiO_2 - K_2O variation diagram of electron microprobe analyses of vitric shards in Holes 836A and 838A. Reference fields for Lau Ridge volcanics from Cole et al. (1985).

hemipelagic sediments. The boundary between the flow units was recognized by a sharp change in the grain size and color of the sediment, associated with a presumed erosive contact. The lower flow unit directly overlies a clayey nannofossil ooze with prominent water-escape structures (e.g., mud diapir).

Three samples from the lower unit (135-837A-6H-5, 22–24 cm [52.28 mbsf], -6H-5, 1–3 cm [52.01 mbsf], and -5H-5, 17–19 cm [42.67 mbsf]) show systematic variations in grain size as well as lithologic and chemical composition. Grain sizes are largest at the base ($Md_\phi = 1.79 \Phi$, 289 μm) and smallest in the upper parts ($Md_\phi = 5.05 \Phi$, 30 μm). Very dark gray to green gray sediments in the lower part are thinly bedded to thickly laminated and are made up of varying proportions of dominantly colorless, highly vesicular pumice clasts, and lesser amounts of pale brown blocky and angular shards of low to medium vesicularity. Some blocky shards show pronounced perlitic cracks and rare trachytic textures. Igneous minerals (plagioclase, hypersthene, clinopyroxene, and opaques), often euhedral, make up <10 vol% of the sediment in the lower part, which has an andesitic bulk composition (61.1–66.6 wt% SiO_2 , 0.51–0.76 wt% K_2O). Igneous minerals are rare farther upsection, where the bulk composition is rhyolitic (74.0 wt% SiO_2 , 1.12 wt% K_2O).

The upper 12 m of the flow unit, very homogeneous and lacking macroscopic sedimentary structures, are made up mostly of colorless bubble junction, bubble wall, and needlelike shards, beside rare colorless pumice clasts.

Sample 135-837A-4H-2, 122–124 cm (29.72 mbsf) ($Md_\phi = 5.16 \Phi$, 28 μm), which was taken about 5 m above the base of the upper flow in Unit II (Hole 837A), is lithologically very similar to the upper sample from the lower flow (135-837A-5H-5, 17–19 cm; 42.67 mbsf). Chemically both samples are almost identical.

We interpret both massive units in Unit II to be emplaced as subaqueous pyroclastic flows from a single major submarine eruptive event because of their compositional and chemical homogeneity. Characteristic trace element ratios such as Ba/Zr (mean 3.77, standard deviation 0.18) and Zr/Y (Mean 2.23, standard deviation 0.17) are constant (Fig. 12). Major and trace element compositions of bulk volcaniclastics are identical. Lithic and tachylitic fragments are absent in both units; rare clasts with trachytic textures may be xenolithic. Andesitic bulk compositions in the lower part are a result of the admixture of more mafic clasts, which were enriched in the lower part of the flow by their higher density and higher settling velocities. They may be accidental/xenolithic, but more likely they indicate eruption

from a chemically zoned magma chamber, considering the small variations of trace element ratios.

A proximal location of the site with regard to the eruptive vent seems likely, because of the large cumulate thickness of both units (>25 m). However, we will discuss below the possible origin from an unusual paroxysmal submarine eruption, and the probable correlation to deposits in Site 839, >50 km away.

Further studies (e.g., electron microprobe, vesicle modes) are required to confirm the interpretation and establish a more detailed model for the eruption and deposition of Unit II in Hole 837A.

Unit III (Hole 837A)

Unit III comprises 26 volcaniclastic layers (mostly 4–21 cm thick), all <0.6 m.y. old, deposited after a hiatus in volcaniclastic input of about 0.8 m.y., during which mostly nannofossil ooze was deposited. Four more prominent layers, 34–102 cm thick can be found in the lower third of the unit. Five primary fallout tephras layers were distinguished. Three samples from the upper 21 m of Hole 837A cover the narrow age span from 0.59 to 0.55 Ma.

1. Sample 135-837A-3H-3, 32–34 cm (20.82 mbsf) ($Md_\phi = 4.78 \Phi$, 36 μm), is from a 145-cm-thick, olive gray to gray, thinly bedded, upward-fining volcaniclastic unit. It is interbedded in clayey nannofossil ooze with an erosional contact at the base.

2. Sample 135-837A-3H-1, 89–91 cm (18.52 mbsf) ($Md_\phi = 2.76 \Phi$, 148 μm), was taken in an olive gray volcaniclastic unit, >1 m thick, at the base of an overall upward-fining volcaniclastic unit that is >5 m thick and erosively overlies nannofossil ooze. Foraminifers make up almost 50 vol% in the coarser fractions.

3. Sample 135-837A-2H-6, 120–122 cm (17.72 mbsf) ($Md_\phi = 5.23 \Phi$, 27 μm), comes from one of numerous upward-fining, light yellowish brown to brownish gray volcaniclastic units, which are mostly <20 cm thick and lack hemipelagic intervals. No internal sedimentary structures occur except for a sharp base and graded top.

A fourth sample, 135-837A-1H-5, 84–86 cm (6.86 mbsf) ($Md_\phi = 4.94 \Phi$, 33 μm) has an estimated age of 0.34 Ma and was taken from a volcaniclastic unit 15 cm thick, with a sharp lower contact to clayey nannofossil ooze, and grading into dark yellowish brown nannofossil ooze upsection.

All four samples are dominated by colorless bubble wall, bubble junction, platy, needle-like and cusped shards, in addition to varying proportions of pumice clasts (dominant and highly vesicular in Samples 135-837A-3H-3, 32–34 cm, and -3H-1, 89–91 cm, and minor pale to medium brown shards that also contain rare pale brown blocky shards with microlites and trachytic texture. Igneous minerals (plagioclase, hypersthene, clinopyroxene, and opaques) make up <1 vol% and reach about 5 vol% in Sample 135-837A-1H-5, 84–86 cm. Brown to green clay minerals are rare, but they are more common in Sample 135-837A-1H-5, 84–86 cm, in which pale brownish zeolites were also found.

All tephras in the four samples above have a rhyolitic bulk composition, with SiO_2 ranging from 71.8 to 74.6 wt%. They overlap with the low-K series, with K_2O ranging from 0.94 to 1.07 wt%, resembling such chemical trends as those found in the Lau Basin basement lavas. Sample 135-837A-3H-1, 89–91 cm, with 0.77 wt% K_2O has closer affinities to the very-low-K series. The Ba/Zr ratios, which increase systematically from 4.27 to 6.06 upsection, are distinctly higher, however, than in basement lavas (Fig. 6). The highly depleted nature of the source is evident from the extremely low Zr concentrations, even in the rhyolites, which are also significantly lower than in the basement lavas (Fig. 13).

All samples from Unit III in Hole 837A are interpreted as turbidite deposits, except for Sample 135-837-1H-5, 84–86 cm, which has characteristics of a fallout layer. The abundance of clay mineral fragments and occurrence of zeolites may, on the other hand, indicate

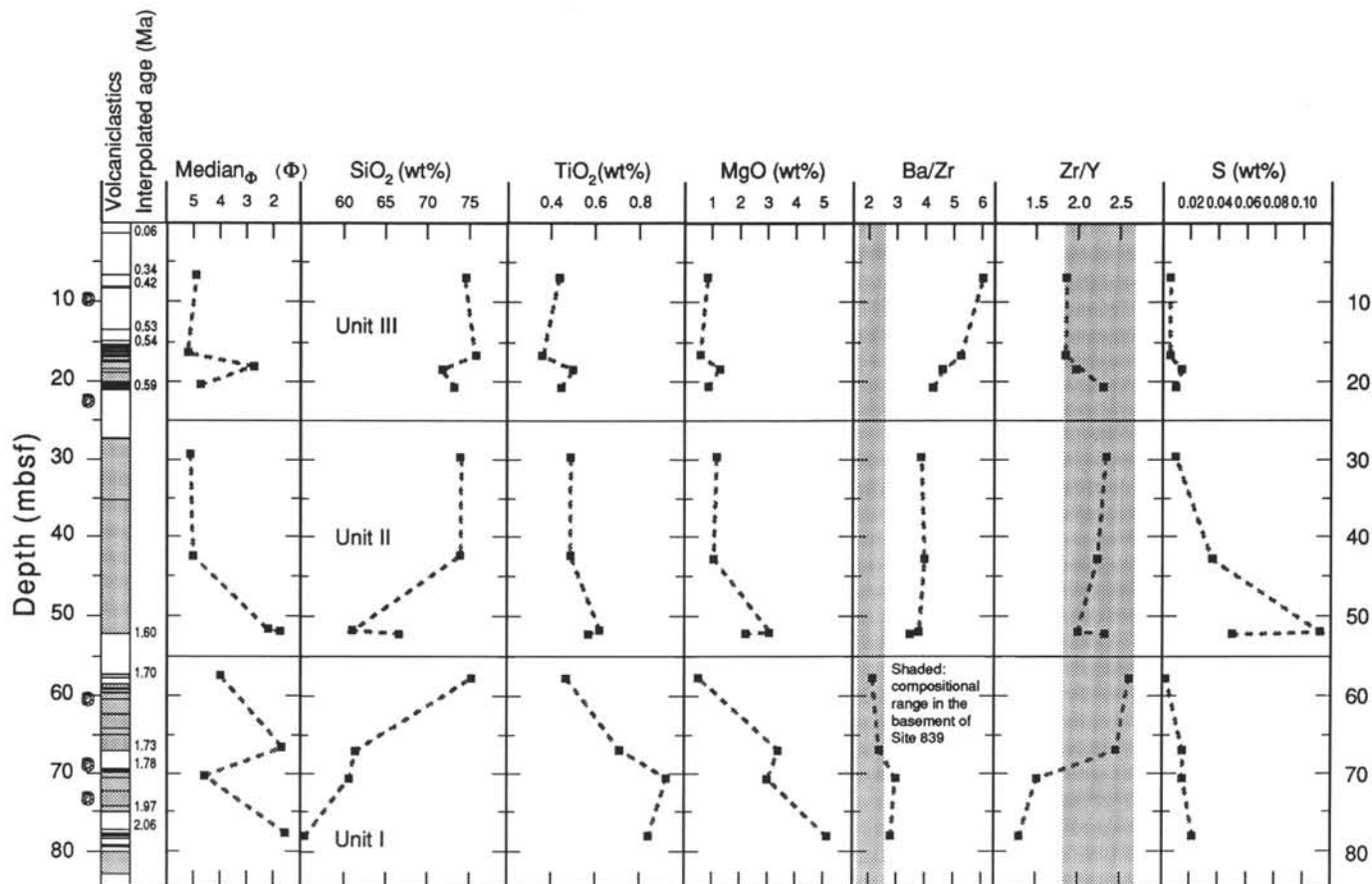


Figure 12. Downhole variations in Md_{Φ} (Φ), SiO_2 (wt%), TiO_2 (wt%), MgO (wt%), Ba/Zr ratio, Zr/Y ratio, and S (wt%) of volcaniclastic bulk-rock samples from Hole 837A. Shaded areas and thin black lines in the schematic columnar section indicate occurrence of volcaniclastic layers. Foraminifer symbol on the left-hand depth column indicates depth of bioevents used to calculate sediment accumulation rates (Parson, Hawkins, Allan, et al., 1992). Ba/Zr and Zr/Y ratios for volcanic basement of Site 839 are shipboard data (Parson, Hawkins, Allan, et al., 1992).

an epiclastic origin. The small grain sizes are consistent with more distant sources of volcaniclastic material found in Units I and II of Hole 837A, reflected also by the decreasing thicknesses of the individual depositional units.

Site 838

Three characteristic units are distinguished in Hole 838A (Fig. 14).

Unit I (Hole 838A)

Unit I in Hole 838A (68.94 to >97.92 mbsf; >1.8 Ma old) is dominated by two thick vitric mass flows, 18 m (MF1) and 4.5 m (MF2) thick (Fig. 14). A 1.20-m-thick, mud-supported volcanic breccia in the upper part of MF1 is interpreted as a slump deposit. Unit I is discriminated from the upper part of Hole 838A by distinctly low and constant Zr/Y and Ba/Zr ratios in the bulk samples. Two samples from each of the major depositional units were studied.

MF1. Samples 135-838A-11H-6, 39–41 cm (97.09 mbsf, 1.92 Ma) ($Md_{\Phi} = -0.78 \Phi$, 1.72 mm), and -11H-1, 132–134 cm (90.52 mbsf), belong to a series of thickly bedded, partially upward-fining, very dark gray volcaniclastic sediments also containing mud clasts of mixed sediment. Farther upsection, this flow becomes generally structureless mixture of grayish pumice clasts (normally <1 cm in diameter, and with maximum diameters of ca. 3 cm) and dense, black, angular vitric clasts resembling hyaloclastites, normally <0.5 cm in diameter. Microscopically, colorless to pale brown pumice shards with low to medium vesicularity dominate clearly. Blocky and platy, pale to medium brown

shards with low to medium vesicularity, often with abundant microlitic, tachylitic, and/or trachytic groundmass, occur throughout the sample. Few clasts are altered to greenish/brownish clay minerals.

In the lower sample of MF1, glass compositions range from 51.1 to 73.9 wt% SiO_2 but are dominantly in the basaltic andesitic and andesitic range. The gradient of K_2O enrichment is very low, reaching about 0.46 wt% K_2O at 70 wt% SiO_2 (Fig. 11). In the more mafic glasses, Al_2O_3 is distinctly lower than in other samples from farther upsection in Hole 838A (Fig. 10). The Ba/Zr ratios in the MF1 bulk-rock samples range from 2.3 to 2.6.

The observed variations in major element composition within MF1 (Fig. 14) are a result of gravitational enrichment of dense mafic clasts in the lower part of the unit and floating of vesicular, evolved clasts and their enrichment in the central and upper parts of the deposit.

MF2. Samples 135-838A-9H-3, 9–12 cm (73.92 mbsf, 1.80 Ma) ($Md_{\Phi} = 1.12 \Phi$, 460 μm) and -9H-2, 139–142 cm (73.09 mbsf) ($Md_{\Phi} = 1.23 \Phi$, 430 μm) have been taken from a black, fine to very coarse volcaniclastic unit, 4.5 m thick. It is crudely divided into portions of finer and coarser grain sizes with steep dips of up to 40° in the upper parts of the unit. It contains a polymict population of intraclasts, such as (1) an elongate, 20-cm-long, yellowish fragment of heavily altered silicic tuff; (2) greenish gray to gray vesicular volcanic clasts altered to varying degrees; (3) a pumice clast altered to greenish clay minerals; and (4) a clast of reddish clay minerals, 10 cm in diameter. These accidental clasts become increasingly abundant in the lower 30 cm of Section 135-838A-9H-3.

Mostly yellowish to pale brown vitric shards with low to medium vesicle contents are dominated by blocky and platy types (with

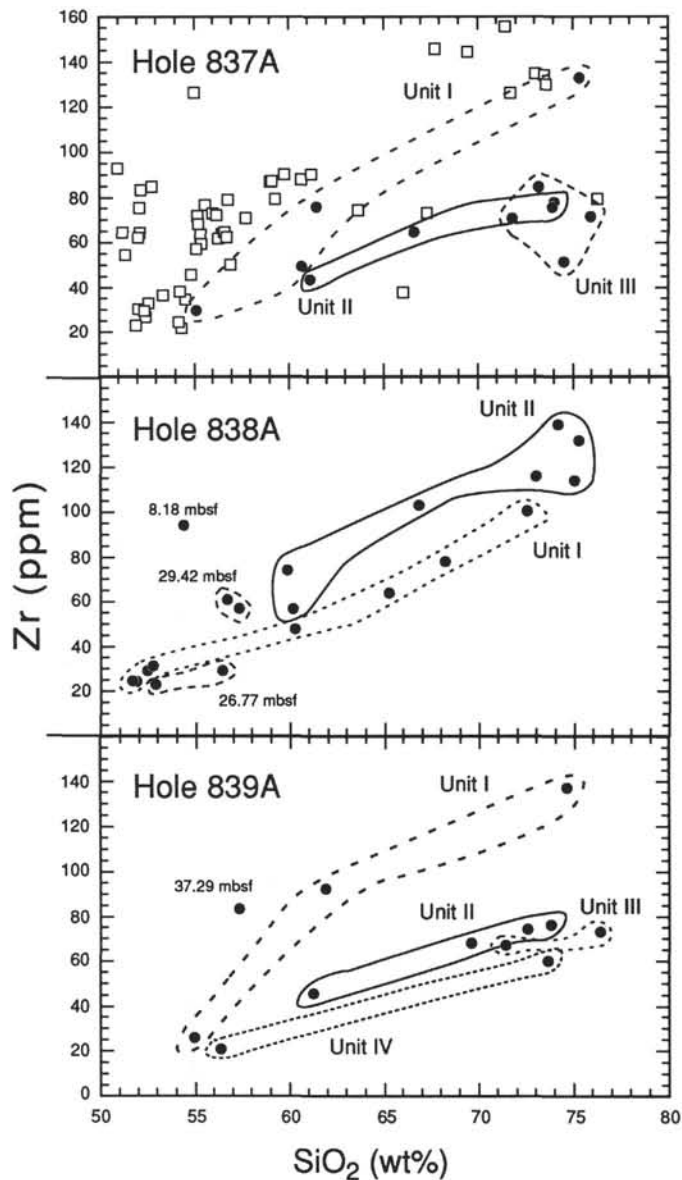


Figure 13. Zr-SiO₂ variation diagram for volcaniclastic bulk rocks in Holes 837A, 838A, and 839A. Open squares in the upper diagram are for compositions of surface samples (mostly taken by TV-grab) from the Lau Basin basement, including Valu Fa Ridge (Sunkel, 1990; G. Sunkel, unpubl. data).

abundant perlitic cracks in the upper sample). Pumice clasts do not occur. Some tachylitic, blocky, angular clasts may have abundant plagioclase microphenocryst. Large crystals and crystal fragments of plagioclase > hypersthene and clinopyroxene reach about 30 vol% at the base of MF2. Alteration is restricted to a few greenish clay mineral fragments and the occurrence of small aggregates of iron hydroxides.

Glasses are basaltic andesites with SiO₂ ranging from 53.0 to 56.7 wt%, at an average K₂O of 0.4 wt%. The average MgO concentration is 6.65 wt%, 1 to 2 wt% higher, as in basaltic andesitic glasses found in the upper part of Hole 835A (Figs. 3 and 5). Ba/Zr ratios from 2.2 to 2.5 match those in MF1.

Large grain sizes of clasts and large thicknesses of deposits are regarded as indicators for a proximal volcanic source for both major depositional units in Unit I of Hole 838A. Thus we favor their origin from a submarine, explosive volcanic eruption. The small variations in characteristic trace element ratios in both MF1 and MF2 implies

their derivation from a single volcanic source, despite an intermittent hemipelagic interval, indicating a hiatus in deposition of volcaniclastics of about 0.1 Ma. Polymict gravels, interpreted as slump deposits, may indicate synvolcanic tectonic activity, however. Steep bedding dips of 30°–40° in this depth range (Parson, Hawkins, Allan, et al., 1992) are in accordance with the possibility that the interlying clay, which is described as inhomogeneous with pebbly intervals, was also emplaced tectonically. In this case, MF1 and MF2 could easily represent products of a single submarine eruption.

Unit II (Hole 838A)

Unit II of Hole 838A (29.29–68.94 mbsf) comprises five major volcaniclastic units, ranging in thickness from 2.3 to 12.4 m, and one thinner layer of volcaniclastic sediments close to the lower boundary of the unit. They were deposited at interpolated ages of about 1 to 1.76 Ma and possess the coarsest grain sizes encountered at any site within the Lau Basin drilled during Leg 135. Unit II is distinguished from Unit I by higher Zr/Y ratios in the bulk samples (Figs. 13–14), whereas Ba/Zr ratios (2.0 to 2.6) remain basically unchanged. All but one of the volcaniclastic units have been sampled for this study.

1. Sample 135-838A-8H-6, 75–76 cm (68.94 mbsf, 1.76 Ma), from a gray volcaniclastic unit, is only 27 cm thick, but it contains highly vesicular pumice clasts in the lapilli size range with a Md_φ of -1.51 Φ (2.85 mm) and maximum clast diameters around 5 cm as dominant components (Fig. 15). This unit, which is reversely graded at the base, is interbedded in homogeneous, brown nanofossil ooze. Colorless to very pale brown pumiceous shards with medium to high vesicularity are the dominant component in thin section, beside some blocky, light brown shards of low to medium vesicularity. Some of the latter have microlitic groundmass textures.

The chemical composition of volcanic glasses is strongly bimodal, with rather magnesian (7 wt% MgO) basaltic andesites ranging from 52.8 to 53.2 wt% SiO₂ and high silica rhyolites with SiO₂ concentrations ranging from 78.3 to 79.7 wt%. The latter follow the LKS and have K₂O concentrations around 1.3 wt%. The distinct and strong increase of FeO/MgO ratios up to 20 in the rhyolite range (Fig. 10) is unique in Hole 838A.

2. Samples 135-838A-7H-6, 46–48 cm (59.16 mbsf, 1.73 Ma); -7H-4, 142–145 cm (57.12 mbsf, 1.73 Ma); and -7H-4, 0–50 cm (56.12 mbsf, 1.73 Ma) have been taken in a coarse-grained, 12.42-m-thick volcaniclastic unit with maximum diameters of pumice clasts around 7 cm and Md_φ values up to -0.73 Φ (1.66 mm), overlying nanofossil ooze. In the lowermost parts, abundant clasts of indurated clay and nanofossil ooze, up to 5 cm in diameter, are found. A similar gravel deposit, 2.28 m thick, with higher proportions of large nonvolcanic clasts such as indurated clays, yellowish ooze, and dark brown to brown ooze (up to 15 cm in diameter), was recovered below volcaniclastic Unit 2, separated only by about 40 cm of clayey nanofossil ooze. Internally, volcaniclastic Unit 2 is widely structureless with some graded layering and upward-fining intervals in the upper third.

In thin section, colorless to very pale brown, highly vesicular pumice shards are most abundant, beside pale brown, low to medium vesicular blocky, bubble junction, and bubble wall shards. Rare tachylitic clasts are angular and have low vesicularity. Among igneous minerals, plagioclase, often euhedral to subhedral, is most abundant. Subhedral to euhedral hypersthene is slightly brownish, and opaques occur mostly as inclusions. Some greenish/brownish clay minerals are found. A thin section from a pumice lapilli from the same depositional unit (Sample 135-838A-8H-1, 137–140 cm), which was studied on board, contains euhedral to slightly corroded quartz phenocrysts and subhedral, greenish to brownish hornblende.

All samples have a homogeneous rhyolitic bulk composition, with SiO₂ ranging from 73.0 to 75.3 wt% at 116 to 129 ppm Zr, and K₂O concentrations of 1.57 to 1.79 wt%.

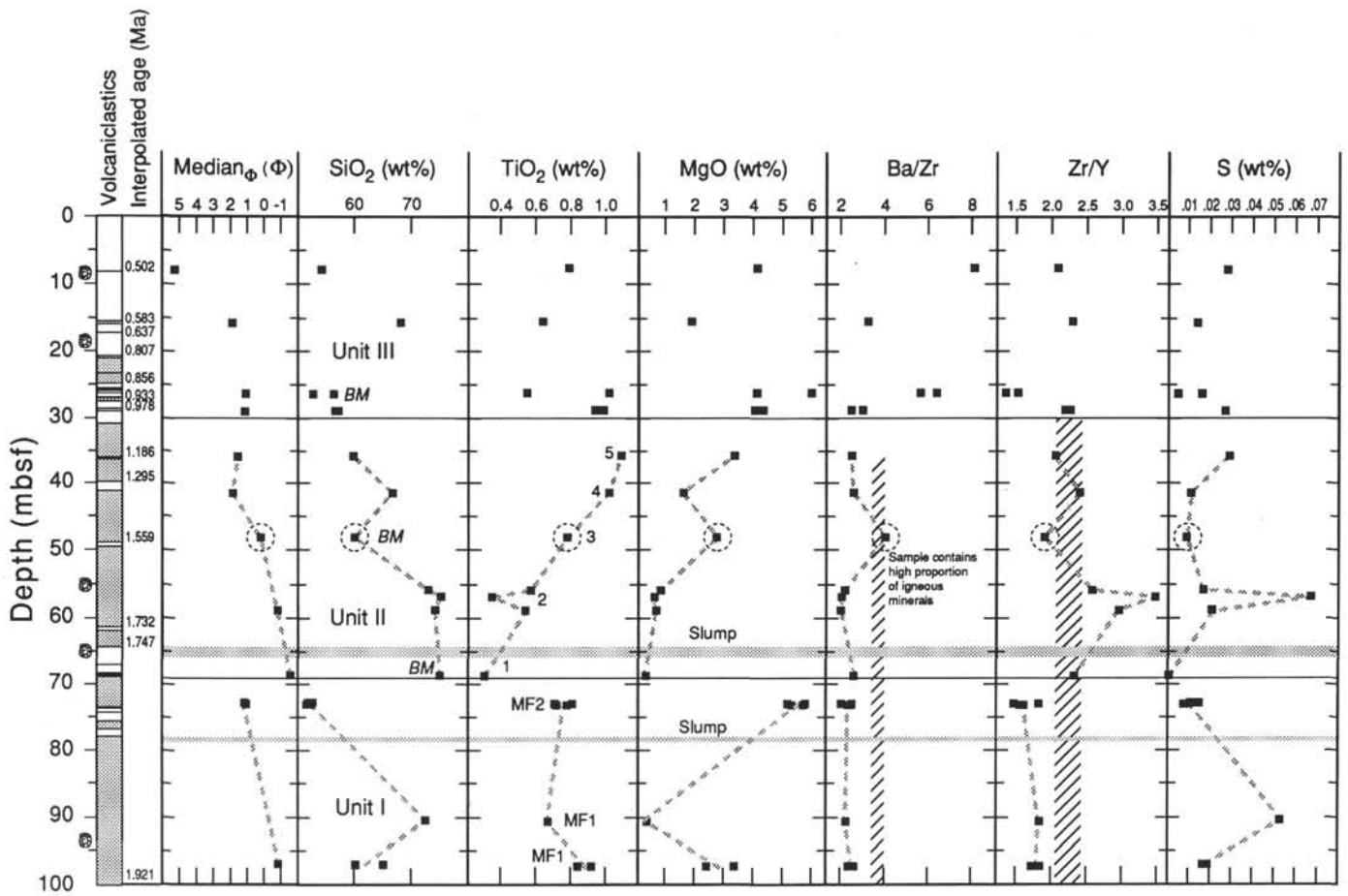


Figure 14. Downhole variation of Md_{Φ} (Φ), SiO_2 (wt%), TiO_2 (wt%), MgO (wt%), Ba/Zr ratio, Zr/Y ratio, and S (wt%) of volcaniclastic bulk rock samples from Hole 838A. Shaded areas and thin black lines in the schematic columnar section indicate the occurrence of volcaniclastic layers. MF1 and MF2 = subunits in Unit I of Hole 838A; 1 to 5 = subunits in Unit II of Hole 838A; BM = samples with bimodal chemical composition of glasses (as measured by electron microprobe). Horizontal gray bars indicate depth of mud-clast-rich layers interpreted as slump breccias. Foraminifer symbol in the left-hand column indicates depth of bioevents used to calculate sediment accumulation rates (Parson, Hawkins, Allan, et al., 1992). Hatched areas in the Ba/Zr and Zr/Y columns indicate compositional spectrum in Unit II of Hole 837A and Unit II of Hole 839A.

3. Sample 135-838A-6H-5, 53–55 cm (48.23 mbsf, 1.56 Ma) (Md_{Φ} = 0.28 Φ , 0.82 mm), comes from a light gray to gray, coarse-grained volcaniclastic deposit, 7.64 m thick, overlying nannofossil ooze with an erosional contact. Maximum pumice diameters reach 4 cm, whereas mud clasts close to the base have diameters up to 15 cm. Internally the unit is mostly structureless; vaguely defined bedding, often with normally graded internals, becomes more abundant upsection.

Colorless and rarely pale brown pumice clasts are the dominant component in thin section, beside blocky and platy, pale brown shards with low to medium vesicularity. The latter often have a microlitic groundmass texture, but no pronounced alignment of microlites. Blocky, angular, tachylitic clasts with low to medium vesicularity are rare. Igneous minerals (mostly complex zoned and cored plagioclase), hypersthene, clinopyroxene, and opaques (mostly as inclusions) make up 50–60 vol%. Some brownish clay minerals and Fe-Mn micronules are found, the latter as isolated grains with layered internal structures and/or coating on some glass shards. Glass composition is bimodal, with the dominant populations from 51.4 to 55.3 and from 75.4 to 80.2 wt% SiO_2 . K_2O is 1.3 to 2.0 wt% in the rhyolite. Bulk-

rock compositions are not discussed because of the high proportion of igneous minerals.

4. Sample 135-838A-5H-7, 40–42 cm (41.60 mbsf, 1.30 Ma) (Md_{Φ} = 1.92 Φ , 260 μm), of dacitic bulk composition (66.8 wt% SiO_2 , 103 ppm Zr, Ba/Zr = 2.6) was taken from a grayish brown, graded, volcaniclastic unit, 355 cm thick, overlying dark brown clayey nannofossil ooze. Colorless to very pale brown pumice shards of medium to high vesicularity make up about 80 vol%. Blocky and platy pale brown shards of medium vesicularity are less abundant. Tachylitic clasts and phenocrysts and microphenocrysts of plagioclase, clinopyroxene, and opaques are rare.

5. Sample 135-838A-5H-3, 88–90 cm (36.08 mbsf, 1.19 Ma) (Md_{Φ} = 1.61 Φ , 330 μm) of andesitic bulk composition (59.8 wt% SiO_2 , 74 ppm Zr, Ba/Zr = 2.51) contains 60–70 vol% colorless to very pale brown/yellowish, low to high vesicularity pumice shards. Blocky and platy, pale to medium brown, low to medium vesicularity shards are less abundant. Clasts with microlitic groundmass texture, and microphenocrysts of hypersthene, clinopyroxene, and opaques are rare. This sample is from a 5.19-m-thick, widely structureless, black volcaniclastic

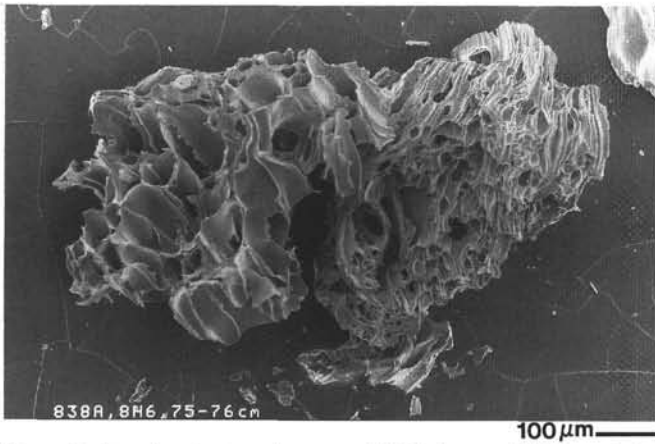


Figure 15. Scanning electron microscope (SEM) picture of highly vesicular rhyolitic pumice clast from Sample 135-838A-8H-6, 75–76 cm (68.94 mbsf), with an estimated age of 1.76 Ma. In the same bed, only 27 cm thick, pumice lapilli reach diameters of up to 5 cm.

layer that is graded in the lower part. Brown mudstone clasts, up to 9 cm in diameter, become increasingly abundant upsection.

Five depositional units studied in Unit II, all separated by thin hemipelagic intervals, show a remarkably systematic variation of bulk-rock major element compositions that become progressively more mafic upsection. The microprobe data of volcanoclastic Units 1 and 2, however, show a strong bimodality of chemical compositions (thin sections from the other samples also show at least two populations of glass shards), so that these systematic variations must be considered as coincidental. Ba/Zr ratios (2.0 to 3.0, except for one sample containing >50 vol% crystals) are almost constant, whereas Zr/Y ratios (2.1 to 3.5) are quite variable (Fig. 14). Absolute Zr concentrations overlap with some of the basement lavas (Fig. 13), but are overall distinctly lower. With the present data, before additional microprobe studies, it is not possible to identify clearly the number of volcanic centers/sources contributing to the deposition of Unit II. The large thicknesses and grain sizes of the volcanoclastics in Unit II, however, suggest proximal sources within the Lau Basin, probably with increasing distance between the source and Site 838 upsection.

Unit III (Hole 838A)

Unit III (<29.29 mbsf, <1 Ma old) comprises about 15 turbidites (up to 2 m thick) and turbidites with vitric-rich bases (<10 cm thick). Four samples cover the age span from 0.93 to 0.50 Ma.

Sample 135-838A-4H-5, 59–61 cm (29.29 mbsf, 0.93 Ma) ($Md_{\phi} = 1.20 \Phi$, 440 μm), of andesitic bulk composition (56.6–57.3 wt% SiO_2 , 57–61 ppm Zr, Ba/Zr = 2.5–3.0), is taken from a 64-cm-thick, black, graded layer of volcanoclastics, overlying dark brown, clayey nannofossil ooze. The shard and clast assemblage is heterogeneous with colorless pumice shards of medium vesicularity, pale yellowish to brownish blocky and platy shards of medium vesicularity, abundant clasts with tachylitic groundmass, and abundant clasts with different degrees of groundmass crystallization (mostly trachytic). Plagioclase, hypersthene, clinopyroxene, and opaques occur predominantly as microphenocrysts. Some clusters and aggregates of greenish-yellowish clay minerals are found.

Sample 135-838A-4H-3, 100–102 cm (26.70 mbsf, 0.86 Ma) ($Md_{\phi} = 1.15 \Phi$, 450 μm), from a grayish brown volcanoclastic unit, 168 cm thick, with prominent water-escape structures in the lowermost part, is also characterized by polymict components. These include colorless, highly vesicular pumice shards; large, low to medium, vesicular pale yellowish brown blocky and platy shards (with abundant perlitic cracks); and a wide range of clasts with different

degrees of groundmass crystallization (mostly trachytic). About 30 vol% of igneous minerals, mostly as isolated euhedral to anhedral grains and glomerophytic clusters are dominantly plagioclase, beside pale brownish hypersthene, pale greenish-pinkish clinopyroxene, and abundant opaque microphenocrysts. Prehnite occurs in lithics with quartz and iron hydroxides.

Glass compositions are strongly bimodal, with SiO_2 ranging from 50.2 to 54.3 wt% and 75.5 to 78.9 wt%. The rhyolites follow the LKS trend with 0.98 to 1.18 wt% K_2O ; the basaltic andesites are rather mafic with up to 7.6 wt% MgO. Note the small variation of bulk-rock trace element ratios in two different grain-size fractions from this sample (Ba/Zr = 5.7 to 6.4), even though major elements show significant variations caused by different proportions of the two shard populations in the different grain-size fractions (Fig. 13).

Sample 135-838A-3H-2, 141–143 cm (16.11 mbsf, 0.58 Ma) ($Md_{\phi} = 1.95 \Phi$, 260 μm), with a dacitic bulk composition (68.2 wt% SiO_2 , 78 ppm Zr, Ba/Zr = 3.3), comes from a laminated, grayish brown volcanoclastic unit, 51 cm thick, interbedded in clayey nannofossil ooze. Abundant colorless, highly vesicular pumice shards, beside pale to medium brown, medium to low vesicular platy shards, only rarely with high aspect ratios, make up the bulk of the sediment. Euhedral to subhedral microphenocrysts of plagioclase and clinopyroxene and small, greenish clay minerals are rare.

Sample 135-838A-2H-3, 147–149 cm (8.18 mbsf, 0.50 Ma) ($Md_{\phi} = 5.33 \Phi$, 25 μm), a heterogeneous sediment of many different clast types and clasts with different degrees of alteration, was taken from a burrow structure in clayey nannofossil ooze. It comprises mostly pale to medium brown, low to medium vesicular platy shards, and rare pale brown pumice shards of medium vesicularity. Some clasts with microlitic fluidal groundmass and plagioclase, hypersthene, clinopyroxene crystals occur. About 10 vol% of altered material includes greenish-brownish clay minerals; pale brown to colorless, fibrous zeolites; and iron hydroxides. Glasses are of andesitic composition with SiO_2 ranging from 56.9 to 59.6 wt%.

Although the thickness of individual volcanoclastic layers decreases, when compared with Unit II in Hole 838A, relative large average grain sizes remain unchanged. As with the units below, we are at present not capable of positively identifying the sources for these layers, but we favor the origin from volcanoes within the Lau Basin.

The uppermost sample of Unit III may be a thin distal fallout layer, ripped-up by bioturbation. The unusual high Ba/Zr ratio (8.1; see Fig. 14) and the high Zr concentrations (Fig. 13) are consistent with a different source than for the other volcanoclastics in Unit III. This probably marks the beginning of explosive volcanism on the Tofua Arc.

Site 839

Three characteristic units were distinguished above 90 mbsf in Hole 839A by sedimentologic and lithologic criteria, and bulk-rock chemistry (Figs. 13 and 16). Downhole, a fourth group was discriminated, mainly because of high Zr values (Fig. 16).

Unit I (Hole 839A)

More than 13 layers rich in volcanoclastics were detected in Unit I, none exceeding 1.11 m in thickness. Below 100 mbsf core recovery was very poor. Extreme sedimentation rates of 882 mm/k.y. (88.2 m in 0.1 m.y.) in this part (Parson, Hawkins, Allan, et al., 1992), imply predominance of proximal volcanoclastic input with great thicknesses of individual depositional units.

Three silt- to sand-sized samples from Unit I (135-839A-21X-CC, 36–38 cm [186.56 mbsf, 1.83 Ma] [$Md_{\phi} = 1.77 \Phi$, 290 μm]; 135-839A-15X-2, 44–46 cm [128.94 mbsf, 1.76 Ma] [$Md_{\phi} = 4.90 \Phi$, 30 μm]; and 135-839A-11H-6, 95–97 cm [98.45 mbsf, 1.73 Ma] [$Md_{\phi} = 2.52 \Phi$, 170 μm]) have bulk compositions ranging from basaltic andesitic to rhyolitic (55.0, 61.9, and 74.7 wt% SiO_2). K_2O concentrations of 1.76 wt% in the rhyolite and 1.03 wt% in the andesite are

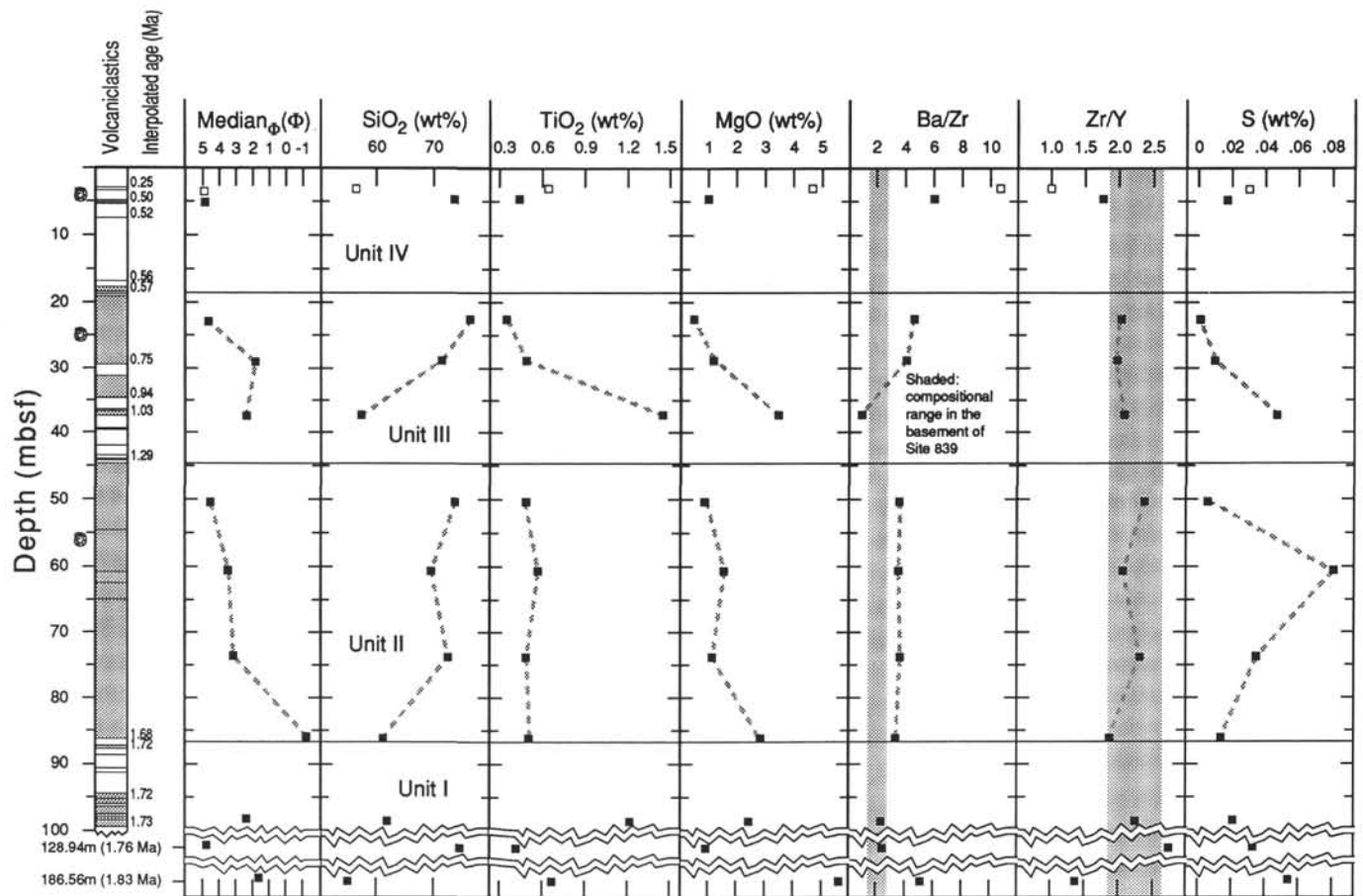


Figure 16. Downhole variations in Md_{Φ} (Φ), SiO_2 (wt%), TiO_2 (wt%), MgO (wt%), Ba/Zr ratio, Zr/Y ratio, and S (wt%) of volcaniclastic bulk-rock samples from Hole 839A. Open symbol indicates sample interpreted as subaerial fallout tephra. Shaded areas and thin black lines in the schematic columnar section indicate the occurrence of volcaniclastic layers. Foraminifer symbol in the left-hand column indicates depth of bioevents used to calculate sediment accumulation rates (Parson, Hawkins, Allan, et al., 1992). Ba/Zr and Zr/Y ratios for volcanic basement at Site 839 are shipboard data (Parson, Hawkins, Allan, et al., 1992).

slightly higher than in the Lau Basin basement LKS. Ba/Zr ratios (2.38 to 2.48) barely overlap with data of basement lavas (Fig. 6) whereas Ba/Zr in the basaltic andesite (5.12) is distinctly higher. Absolute Zr concentrations in Unit I are closest to trends of the Lau Basin basement (Fig. 13), when compared with the other volcaniclastics in Hole 839A. Ba/Zr ratios are somewhat higher, however. The trace element characteristics of Unit I (Hole 839A) are strikingly similar to those of Unit I (Hole 837A) (Figs. 12–13 and 16).

Unit II (Hole 839A)

Unit II (44.0–87.7 mbsf), almost completely free of hemipelagic intervals, is made up of seven vitric turbidites and pumiceous vitric grain flows, which are up to 21.3 m thick and average around 6 m in thickness.

Three samples from Unit II (135-839A-9H-2, 129–131 cm [73.79 mbsf] [Md_{Φ} = 3.29 Φ , 102 μ m]; 135-839A-7H-6, 129–131 cm [50.42 mbsf] [Md_{Φ} = 3.60 Φ , 82 μ m]; and 135-839A-6H-6, 42–44 cm [50.42 mbsf] [Md_{Φ} = 4.66 Φ , 40 μ m]) have a homogeneous, rhyolitic bulk composition (69.6–73.8 wt% SiO_2 , 0.88–1.04 wt% K_2O). In the gray, soupy sediment all internal structures were destroyed by drilling. It is made up dominantly by mostly colorless and highly vesicular, partially yellowish to medium brown pumice clasts of medium vesicularity. Blocky medium brown shards with lower vesicularity and brownish clasts with groundmass microlites and trachytic textures are rare. The total phenocryst mode is up to 2 vol% (plagioclase, rare clinopyroxene, and opaques).

A fourth sample (135-839A-10H-4, 102–104 cm) from the base of the lowermost, 21.30-m-thick depositional unit in Unit II, has an andesitic bulk composition (61.25 wt% SiO_2 , 0.57 wt% K_2O). It is described as a light gray to very dark gray volcaniclastic sediment, dominated by pumiceous clasts and black, angular, hyaloclastite-like fragments that are most abundant in the lowermost 25 cm, erosionally overlying nannofossil ooze. In thin section, colorless, mostly highly vesicular pumice clasts are more abundant than pale yellowish brown to light brown shards with low vesicularity, which mostly have a trachytic texture. Some blocky and angular tachylitic clasts are found. Detrital altered fragments include clasts of chlorite(?)–quartz(?)–opaques–iron hydroxide, greenish/brownish clay minerals, and Fe–Mn micronodules. Phenocrysts make about 40 vol% (plagioclase > hypersthene – clinopyroxene – opaques [mostly as inclusions]).

We interpret Unit II to be produced by a single eruption mainly because of relatively constant characteristic trace element ratios (Fig. 16) and the lack of interbedded, hemipelagic intervals. Assuming that the whole sequence was deposited almost instantaneously the best age estimate for the eruption would be that of the bioevent (last appearance datum *G. oceanica*) found at 56 mbsf in the upper third of Unit II (1.68 Ma). This assumption modifies the sediment accumulation rates considerably and also increases the interpolated depositional ages above Unit II by up to about 0.4 Ma.

The great thickness and large grain sizes of volcaniclastics are likely to indicate a proximal, deep submarine source. The andesitic bulk composition in the lower part of the lower flow in Unit II is

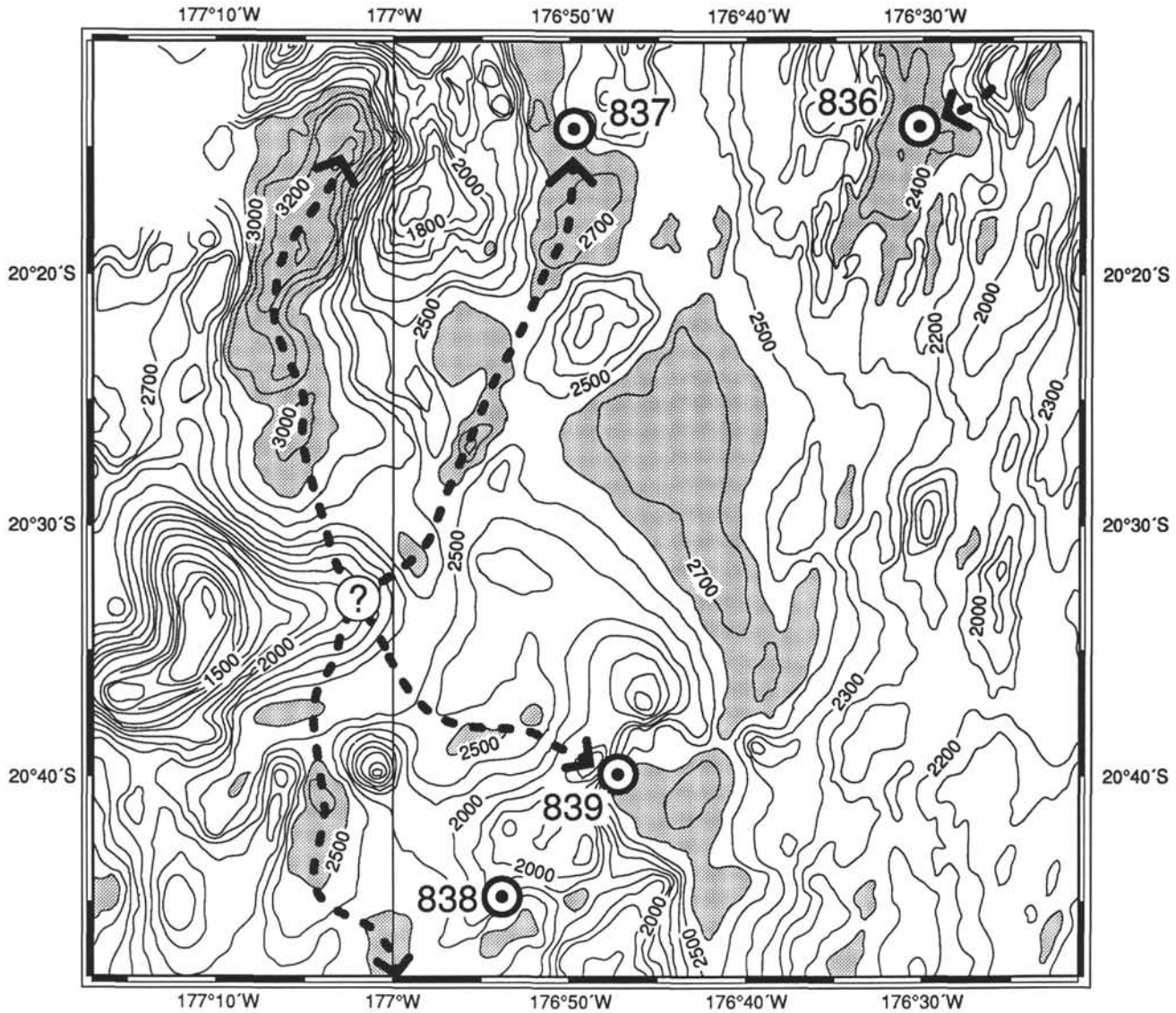


Figure 17. Bathymetric chart of the southern Lau Basin showing the locations of Sites 836–839 and the potential pathways for hyaloclastite deposition (Site 836) and mass flows depositing Unit II of Hole 837A and Unit II of Hole 839A. Bathymetry redrawn after Parson et al. (1992). Contour intervals are in meters.

interpreted to be a result of gravitational enrichment of denser, more mafic clasts. Before further detailed microprobe studies, we can only suspect that the mafic shards may be caused by an eruption from a zoned magma chamber. Altered clasts and those with crystalline groundmass textures are xenolithic.

Unit II in Hole 839A correlates strikingly well with Unit II in Hole 837A in major and trace elements (Figs. 12–13 and 16) and in interpolated ages (1.6–1.7 Ma). Even with the present limited knowledge about the location of the eruptive site(s), eruption mechanisms, primary and secondary dispersal patterns and deposition of tephra we find a direct correlation over a distance >50 km is a feasible assumption (see also Figs. 1–2). For instance, if the eruption had occurred on the western flank of the large seamount, located at about 20°40'S, 177°10'E (Fig. 17), excellent pathways existed to both directions (Sites 837 and 839). A larger distance for Unit II in Hole 837A to the source when compared to Unit II in Hole 839A is consistent with the thicknesses and grain sizes of the deposits (Table 4). Site 838, where we could not yet identify an equivalent to this unit (see also Fig. 14) would have been sheltered from direct input by at least two smaller

Table 4. Comparison of important chemical and sedimentological characteristics of Unit II (Hole 837A) and Unit II (Hole 839A).

	Hole 837A Unit I	Hole 839A Unit II
Estimated age (Ma)	1.60	1.68
Rhyolite composition:		
Zr/Y	2.23-2.33	2.06-2.38
Ba/Zr	3.89-3.99	3.57-3.69
FeO ⁰ /MgO	3.03-3.33	2.9-3.7
K ₂ O (wt%)	1.12-1.13	0.88-1.04
Sedimentological characteristics:		
Maximum grain-size at base (mm)	5	30
Median grain-size at base (μm)	283	102
Median grain-size in upper part (μm)	28 - 30	40
Total thickness of unit (m)	25.18	43.70

seamounts and a small, approximately east-trending bathymetric ridge (Fig. 17). We expect lateral and radial thickness distributions of the deposits to resemble those of subaerial, channelized pyroclastic flows rather than fallout tephra, where thicknesses of deposits may be orders of magnitude higher within topographic lows than on directly neighboring slopes and hills. Even thicker deposits of this eruption may probably be found in a basin >300 m deep directly to the north of the seamount.

Unit III (Hole 839A)

Unit III (18–44 mbsf, 0.6–1.3 Ma) is made up of >10 vitric turbidites, turbidites with vitric rich bases, and some fallout tephra.

Sample 135-839A-5H-3, 129–131 cm (37.29 mbsf, 1.03 Ma) ($Md_{\phi} = 2.52 \Phi$, 174 μm), has an andesitic bulk composition (57.3 wt% SiO_2 , 0.48 wt% K_2O , $\text{Ba}/\text{Zr} = 0.98$) and was taken from a 64-cm-thick gray volcanoclastic unit. Vitric shards are dominated by blocky and platy, medium brown, rarely dark brown angular fragments mostly with low vesicularity and perlitic cracks.

Samples 135-839A-4H-4, 110–112 cm (29.10 mbsf, 0.75 Ma) ($Md_{\phi} = 1.98 \Phi$, 250 μm), and -3H-6, 140–142 cm (22.90 mbsf) ($Md_{\phi} = 4.78 \Phi$, 36 μm), were taken from a light to dark brownish gray, rhyolitic volcanoclastic deposit, 10.28 m thick. Maximum pumice diameters in this upward-fining sequence reach about 3 cm at the base. The chemical bulk composition is rather homogeneous with 71.4–76.4 wt% SiO_2 and a Ba/Zr ratio of 4.10 to 4.64. K_2O concentrations (0.78 wt% and 0.94 wt%) are slightly lower than in the LKS.

Unit IV (Hole 839A)

Unit IV (<10 mbsf) comprises less than ten beds of volcanoclastics, which do not exceed 11 cm in thickness.

One rhyolitic sample (135-839A-2H-1, 39–41 cm [4.89 mbsf, 0.50 Ma] [$Md_{\phi} = 5.00 \Phi$, 30 μm]), with 73.7 wt% SiO_2 , 1.06 wt% K_2O , and $\text{Ba}/\text{Zr} = 6.02$, represents a 9-cm-thick grayish brown sandy unit grading into clayey nannofossil ooze. It comprises mostly bubble junction, bubble wall, and needlelike shards which are mostly colorless, and, more rarely slightly yellowish. A few light to medium brown, blocky, angular shards have a slightly microlitic groundmass. Dirty tachylitic fragments and clayish, yellowish to brownish agglomerates are rare.

A basaltic andesite (Sample 135-839A-1H-3, 30–32 cm [3.30 mbsf, 0.37 Ma] [$Md_{\phi} = 5.05 \Phi$, 30 μm]), with a bulk composition of 56.4 wt% SiO_2 and a high Ba/Zr ratio of 10.2, appears as a discontinuous layer, 4 cm thick, and only slightly grayer as the dark yellowish brown host clay. It is interpreted as an altered, relic ash layer.

DISCUSSION

Only minor contributions to the volcanoclastic record were found from the margins of the Lau Basin (Tofua Arc, Lau Ridge) throughout the Leg 135 sites drilled in the western Lau Basin. We think that most of the volcanoclastic deposits studied resulted from explosive submarine eruptions of mostly rhyolitic magmas from within the basin for the following reasons.

1. The great thickness and large maximum grain sizes of deposits in the lower parts of Sites 837, 838, and 839, and the high sedimentation rates reaching a maximum of 882 mm/k.y. below 100 mbsf in Hole 838A for an interval of about 100 m thickness, are very strong evidence for local volcanic sources. This argument is strengthened by the scarcity of volcanoclastics in Holes 834A and 835A. Though these sites are very close to the Tonga Ridge, which was still active during the opening of the Lau Basin, volcanoclastics make up only 2%–12% of the total sediment.

Abundant geochemical, sedimentological, and volcanological criteria collectively indicate that Unit II in Hole 837A and Unit II in Hole 839A were formed as subaqueous pyroclastic flows from a single

submarine eruption. This correlation necessitates predominant north-south transport.

2. This correlation is in agreement with the assumption that east-west transport by mass flows and/or subaqueous pyroclastic flows is restricted because of the pronounced north-south oriented tectonic fabric of the Lau Basin.

3. Subaerial volcanoes on the Tofua Arc today are rare (reflected in the scarcity of reference data) and widely spaced; they have erupted mostly mafic to intermediate magmas (Bryan et al., 1972; Ewart et al., 1977; Vallier, Stevenson, and Scholl, 1985). The total island volumes are small and it is unlikely that the Tofua Arc was much larger before as it did not even exist before 3 m.y. ago (Hawkins et al., 1984; J. Gill, pers. comm., 1992). Although low-K, high-silica rhyolites dominate the volcanoclastic record in the central Lau Basin (Sites 837–839), little evidence is present for eruptions of highly differentiated magmas, except for some pumice dredged in the Tofua Arc at 23°18'S, 175°30'W (Hawkins, 1985). Pumice from the 1967–1969 eruption on Metis Shoal has a dacitic bulk composition (Ewart et al., 1973).

4. Many volcanoclastics from the Lau Basin sites have Ba/Zr ratios higher than those from the Lau Basin basement lavas. Units I of Hole 837A and of Hole 839A, and Units I and II of Hole 838A, however, overlap considerably in Ba/Zr ratios with shipboard data from the basement of Site 839, which has the strongest "arc signature" of all basement lavas (Figs. 12–14 and 16) (Parson, Hawkins, Allan, et al., 1992; Ewart et al., this volume). Furthermore, all volcanoclastics (except for the arc-derived Korobasaga Group volcanoclastics and high K-calc-alkaline fallout tephra in Hole 834A) have $\text{K}_2\text{O}/\text{H}_2\text{O}$ ratios <0.7 (Fig. 7), characteristic of backarc basin lavas (Saunders and Tarney, 1991).

In the recent past, increasing evidence has been collected for deep submarine explosive eruptions of basaltic to rhyolitic magmas, mainly in subduction-related settings, where even mafic magmas are characterized by high water contents (e.g., Muenow et al., 1990; Gill et al., 1990; Iizasa et al., 1992). Low-K rhyolitic pumice with vesicle contents of 80–85 vol%, dredged from a depth of 3600 m in the Mariana Trough backarc basin, have been attributed to a local source (Lonsdale and Hawkins, 1985). Basalts are reported to have been explosively erupted at a water depth >1800 m from the backarc rift behind the Bonin Arc (Gill et al., 1990). Thick deposits of rhyolitic pumice in the Sumisu Rift area (Sites 788, 790, and 791 of Leg 126) are also interpreted to result partially from deep submarine eruptions (Nishimura et al., 1991). Pumice blocks, several decimeters in diameter, have been repeatedly dredged from seamounts and other locations in the Lau Basin (U. von Rad, pers. comm., 1992). These observations are in agreement with theoretical considerations that deep submarine rhyolitic eruptions are possible at depths exceeding 2000 m (McBirney, 1963; Kokelaar, 1986). They may, however, be limited by the critical pressure of seawater, which is around 0.315 kbar (3150 m water depth, Cas and Wright, 1987). Explosive eruptions of rhyolitic magmas with high H_2O concentrations are thus generally possible throughout the Lau Basin with increasing likelihood and explosivity at decreasing water depths (e.g., seamounts). The solubility of H_2O in rhyolitic melts rapidly decreases when rising through the upper crust. About 6 wt% H_2O may be dissolved at 2 kbars, but only around 1 wt% at 2000 m below sea level (Burnham, 1975; Stolper, 1982).

We favor seamounts as the most likely sites for explosive eruptions in the Lau Basin because the effectiveness of pyroclastic processes strongly increases with the reduction of hydrostatic pressure (Fisher and Schmincke, 1984) and because seamounts provide increased crustal thicknesses, which makes it easier to host magma chambers that may develop rhyolitic magmas. The rarity of dacitic to rhyolitic rocks in the basement (except for the Valu Fa Ridge) does not necessarily mean, however, that those magmas did not evolve at the spreading centers. They just may be rare, and almost exclusively explosively dispersed, rather than of effusive origin.

The volcanoclastics recovered from the Lau Basin are characterized by a high variability of chemical compositions. All bulk compo-

sitions from Sites 837, 838, and 839 possess arc signatures in terms of Ba/Zr ratios that normally increase upsection and range from about 2 to 4, although values >5 are only found in thin volcanoclastic layers <0.6 m.y. old. Even assuming that the young tephra with highest Ba/Zr ratios represent subaerial fallout deposits and distal turbidites from the Tofua Arc, this is still in contrast with observations from the basement of the modern Lau Basin, where, before the drilling of Site 839, a similar arc signature was only known from the youngest crust near the southernmost propagating tip of the Lau Basin (Valu Fa Ridge). At present, we can only speculate that seamounts, the most likely eruptive sites for the submarine explosive tephra, may have different magmatic sources and/or source components than the bulk of the Lau Basin magmas that formed the basement. We find no simple correlation of Ba/Zr ratios with K₂O concentrations and respective enrichment trends (e.g., LKS and VLKS).

Although all volcanoclastics are more depleted in Zr than most lavas from the Lau Basin basement (Fig. 13) large variations of absolute Zr concentrations exist for given degrees of differentiation in the bulk samples, ranging for instance from <60 to >180 ppm at 75 wt% SiO₂. In Holes 837A and 839A, a systematic decrease in Zr concentrations is present at equal degrees of differentiation upsection with the lowest values in Unit III of Hole 837A and Unit IV of Hole 839A and the highest values in Unit I of Hole 837A and Unit I of Hole 839A. This is opposite to the behavior in Hole 838A, which has higher Zr concentrations in Unit II than in Unit I. In the youngest interval, Unit III of Hole 838A, the most enriched as well as the most depleted samples occur (Fig. 13).

With the present limited set of microprobe data, and lacking high-quality trace element analyses of selected bulk samples, any petrologic model for the evolution of the volcanoclastics would be highly speculative. It seems clear, however, that the variations observed reflect the complexity of petrogenetic processes in supra-subduction settings and the abundance of source components, which all might have contributed to the magma generation in the Lau Basin, such as the two mantle components identified by Hergt and Hawkesworth (this volume)—“depleted” Pacific Ocean asthenosphere, and “enriched” Indian Ocean asthenosphere—in addition to other components such as LILE-enriched fluids from the subducted slab, and/or LREE-enriched magmas from partial melting of the subducted slab, and partial melting/assimilation of old arc crust (which may also be present as tectonic fragments within the Lau Basin).

ACKNOWLEDGMENTS

J. Bernhardt, Zentrale Elektronenmikroskopie, Ruhr-Universität Bochum, generously made microprobe time available. Manfred Martini and Thomas Schlüter carefully cleaned and sieved the samples and prepared them for chemical analyses. Kerstin Wolff produced the glass beads for X-ray fluorescence and ran the infrared spectrometers. Tony Ewart provided samples from Metis Shoal and the 1939 Fonulai Island eruption. We thank J. Gill for helpful comments and a review of the manuscript at an earlier stage. Careful reviews by U. von Rad, K. Hoernle, and J. Hawkins improved the manuscript. This work was supported by grants from the Deutsche Forschungsgemeinschaft.

REFERENCES*

- Berggren, W.A., Kent, D.V., and Van Couvering, J.A., 1985. The Neogene: Part 2. Neogene geochronology and chronostratigraphy. In Snelling, N.J. (Ed.), *The Chronology of the Geological Record*. Geol. Soc. London Mem., 10:211–260.
- Bryan, W.B., Stice, G.D., and Ewart, A., 1972. Geology, petrography and geochemistry of the volcanic islands of Tonga. *J. Geophys. Res.*, 77:1566–1585.
- Burnham, C.W., 1975. Waters and magmas: a mixing model. *Geochim. Cosmochim. Acta*, 39:1077–1084.
- Cas, R.A.F., and Wright, J.V., 1987. *Volcanic Successions: Modern and Ancient*. London (Allen & Unwin).
- Cawood, P.A., 1985. Petrography, phase chemistry and provenance of volcanogenic debris from the southern Tonga Ridge: implications for arc history and magmatism. In Scholl, D.W., and Vallier, T.L. (Eds.), *Geology and Offshore Resources of Pacific Island Arcs—Tonga Region*. Circum-Pac. Council. Energy Miner. Resour., Earth Sci. Ser., 2:149–170.
- Churkin, M., Jr., and Packham, G.H., 1973. Volcanic rocks and volcanogenic constituents in sediments, Leg 21, Deep Sea Drilling Project. In Burns, R.E., Andrews, J.E., et al., *Init. Repts. DSDP*, 21: Washington (U.S. Govt. Printing Office), 481–493.
- Cole, J.W., Gill, J.B., and Woodhall, D., 1985. Petrologic history of the Lau Ridge, Fiji. In Scholl, D.W., and Vallier, T.L. (Eds.), *Geology and Offshore Resources of Pacific Island Arcs—Tonga Region*. Circum-Pac. Council. Energy Miner. Resour., Earth Sci. Ser., 2:379–414.
- Cunningham, J.K., and Anscombe, K.J., 1985. Geology of 'Eua and other islands, Kingdom of Tonga. In Scholl, D., and Vallier, T. (Eds.), *Geology and Offshore Resources of Pacific Island Arcs—Tonga Region*. Circum-Pac. Council. Energy Miner. Resour., Earth Sci. Ser., 2:221–258.
- Ewart, A., Brothers, R.N., and Mateen, A., 1977. An outline of the geology and geochemistry, and the possible petrogenetic evolution of the volcanic rocks of the Tonga–Kermadec–New Zealand island arc. *J. Volcanol. Geotherm. Res.*, 2:205–250.
- Ewart, A., Bryan, W.B., and Gill, J., 1973. Mineralogy and geochemistry of the younger volcanic islands of Tonga, southwest Pacific. *J. Petrol.*, 14:429–465.
- Ewart, A., and Stipp, J.J., 1968. Petrogenesis of the volcanic rocks of the central North Island, New Zealand, as indicated by study of ⁸⁷Sr/⁸⁶Sr ratios, and Sr, Rb, K, U, and Th abundances. *Geochim. Cosmochim. Acta*, 32:699–736.
- Exon, N.F., Herzer, R.H., and Cole, J., 1985. Mixed volcanoclastic and pelagic sedimentary rocks from the Cenozoic southern Tonga platform and their implications for petroleum potential. In Scholl, D.W., and Vallier, T.L. (Eds.), *Geology and Offshore Resources of Pacific Island Arcs—Tonga Region*. Circum-Pac. Council. Energy Miner. Resour., Earth Sci. Ser., 2:75–107.
- Fisher, R.V., and Schmincke, H.-U., 1984. *Pyroclastic Rocks*. New York (Springer-Verlag).
- Gill, J., Torssander, P., Lapiere, H., Taylor, R., Kaiho, K., Koyama, M., Kusakabe, M., Aitchison, J., Cisowski, S., Dadey, K., Fujioka, K., Klaus, A., Lovell, M., Marsaglia, K., Pezard, P., Taylor, B., and Tazaki, K., 1990. Explosive deep water basalt in the Sumisu backarc rift. *Science*, 248:1214–1217.
- Gill, J.B., 1970. Geochemistry of Viti Levu, Fiji, and its evolution as an island arc. *Contrib. Mineral. Petrol.*, 27:179–203.
- Hawkins, J.W., 1976. Petrology and geochemistry of basaltic rocks of the Lau Basin. *Earth Planet. Sci. Lett.*, 28:283–297.
- , 1985. Low-K rhyolitic pumice from the Tonga ridge. In Scholl, D.W., and Vallier, T.L. (Eds.), *Geology and Offshore Resources of Pacific Island Arcs—Tonga Region*. Circum-Pac. Council. Energy Miner. Resour., Earth Sci. Ser., 2:171–178.
- Hawkins, J.W., Bloomer, S.H., Evans, C.A., and Melchior, J.T., 1984. Evolution of intra-oceanic arc-trench systems. *Tectonophysics*, 102:175–205.
- Iizasa, K., Yuasa, M., and Yokata, S., 1992. Mineralogy and geochemistry of volcanogenic sulfides from the Myojinsho caldera, the Shichito-Iwojima Ridge, Izu-Ogasawara Arc, northwestern Pacific. *Mar. Geol.*, 108:39–58.
- Kokelaar, B.P., 1986. Magma-water interactions in subaqueous and emergent basaltic volcanics. *Bull. Volcanol.*, 48:275–290.
- Leg 135 Shipboard Science Party, 1991. A new view of ARC/BACKARC systems. *Geotimes*, 36:19–20.
- Lonsdale, P., and Hawkins, J.W., Jr., 1985. Silicic volcanism at an off-axis geothermal field in the Mariana Trough back-arc basin. *Geol. Soc. Am. Bull.*, 96:940–951.
- McBirney, A.R., 1963. Factors governing the nature of submarine volcanism. *Bull. Volcanol.*, 26:455–468.
- Melson, W.G., Jarosewich, E., and Lundquist, C.A., 1970. Volcanic eruption at Metis Shoal, Tonga, 1967–1968. Description and petrology. *Smithson. Contrib. Earth Sci.*, 4.
- Muenow, D.W., Garcia, M.O., Aggrey, K.E., Bednarz, U., and Schmincke, H.-U., 1990. Volatiles in submarine glasses as a discriminant of tectonic origin: application to the Troodos ophiolite. *Nature*, 343:159–161.

* Abbreviations for names of organizations and publication titles in ODP reference lists follow the style given in *Chemical Abstracts Service Source Index* (published by American Chemical Society).

- Nishimura, A., Marsaglia, K.M., Rodolfo, K.S., Collela, A., Hiscott, R.N., Tazaki, K., Gill, J.B., Janecek, T., Firth, J., Isminger-Kelso, M., Herman, Y., Taylor, R.N., Taylor, B., Fujioka, K., and Leg 126 Scientific Party, 1991. Pliocene-Quaternary submarine pumice deposits in the Sumisu rift area, Izu-Bonin arc. In Fisher, R.V., and Smith, G.A. (Eds.), *Sedimentation in Volcanic Settings*. Spec. Publ.—Soc. Econ. Paleontol. Mineral., 45:201–208.
- Parson, L., Hawkins, J., Allan, J., et al., 1992. *Proc. ODP, Init. Repts.*, 135: College Station, TX (Ocean Drilling Program).
- Parson, L.M., Hawkins, J.W., and Hunter, P.M., 1992. Morphotectonics of the Lau Basin seafloor—implications for the opening history of backarc basins. In Parson, L., Hawkins, J., Allan, J., et al., *Proc. ODP, Init. Repts.*, 135: College Station, TX (Ocean Drilling Program), 81–82.
- Riech, V., 1990. Calcareous oozes, volcanic ashes and metalliferous sediments in the Quaternary of the Lau and North Fiji Basins. *Geol. Jahrb., Reihe D*, 92:109–162.
- Riech, V., Marchig, V., Sunkel, G., and Weiss, W., 1990. Hydrothermal and volcanic input in sediments of the Lau Back-Arc Basin, SW Pacific. *Mar. Min.*, 9:183–202.
- Saunders, A., and Tarney, J., 1991. Back-arc basins. In Floyd, P.A. (Ed.), *Oceanic Basalts*: New York (Van Nostrand Reinhold), 219–263.
- Shane, P.A.R., and Frogatt, P.C., 1991. Glass chemistry, paleomagnetism, and correlation of middle Pleistocene tuffs in southern North Island, New Zealand, and Western Pacific. *N.Z. J. Geol. Geophys.*, 34:203–211.
- Smith, I.E.M., Chappell, B.W., Ward, G.K., and Freeman, R.S., 1977. Peralkaline rhyolites associated with andesitic arcs of the southwest Pacific. *Earth Planet. Sci. Lett.*, 37:230–236.
- Stolper, E., 1982. The speciation of water in silicate melts. *Geochim. Cosmochim. Acta*, 46:2609–2620.
- Sunkel, G., 1990. Origin of petrological and geochemical variations of Lau Basin lavas (SW Pacific). *Mar. Min.*, 9:205–234.
- Vallier, T.L., O'Connor, R.M., Scholl, D.W., Stevenson, A.J., and Quintero, P.J., 1985. Petrology of rocks dredged from the landward slope of the Tonga Trench: implications for middle Miocene volcanism and subsidence of the Tonga Ridge. In Scholl, D., and Vallier, T.L. (Eds.), *Geology and Offshore Resources of Pacific Island Arcs—Tonga Region*. Circum-Pac. Council. Energy Miner. Resour., Earth Sci. Ser., 2:109–120.
- Vallier, T.L., Stevenson, A.J., and Scholl, D.W., 1985. Petrology of igneous rocks from Ata Island, Kingdom of Tonga. In Scholl, D., and Vallier, T. (Eds.), *Geology and Offshore Resources of Pacific Island Arcs—Tonga Region*. Circum-Pac. Council. Energy Miner. Resour., Earth Sci. Ser., 2:301–316.
- von Rad, U., Frenzel, G., and Mühe, R., 1990. Origin and alteration of submarine volcanoclastic rocks from the Lau and North Fiji Basins (SW Pacific, SO-35 Cruise). *Geol. Jahrb., Reihe D*, 92:341–393.
- von Rad, U., and Mühe, R., 1990. Mineralogy, chemical composition and origin of ash layers and pumice in sediments from the Lau and North Fiji Basins (SW Pacific, SO-35 Cruise). *Geol. Jahrb., Reihe D*, 92:279–339.
- Whelan, P.M., Gill, J.B., Kollman, E., Duncan, R., and Drake, R.E., 1985. Radiometric dating of magmatic stages in Fiji. In Scholl, D., and Vallier, T. (Eds.), *Geology and Offshore Resources of Pacific Island Arcs—Tonga Region*. Circum-Pac. Council. Energy Miner. Resour., Earth Sci. Ser., 2:415–440.
- Woodhall, D., 1985. Geology of the Lau Ridge. In Scholl, D., and Vallier, T.L. (Eds.), *Geology and Offshore Resources of Pacific Island Arcs—Tonga Region*. Circum-Pac. Council. Energy Miner. Resour., Earth Sci. Ser., 2:351–378.

Date of initial receipt: 18 June 1992

Date of acceptance: 5 April 1993

Ms 135SR-101